Coupled Optoelectronic Oscillator based on Mode-locking Laser for 5G Wireless Networks and Beyond

Lei Zou

A thesis submitted to UCL for the degree of

Master of Philosophy (Mphil)

Department of Electronic and Electrical Engineering

University College London

February 2024

Statement of originality

I, Lei Zou, confirm that the work presented in this thesis is my own. Where information has been derived from other sources, I confirm that this has been indicated in the thesis.

Signed: Lei Zou

.....

Date: 07/02/2024

.....

Abstract

As the microwave signal processing by photonic techniques, the microwave photonic emerge numerous distinct advantages including ultra-high-frequency, large bandwidth, anti-electromagnetic field interference and low transmission loss. As a representative microwave photonic system, the optoelectronic oscillator (OEO) that can generate the radio frequency (RF) signals with excellent performance in terms of phase noise, oscillating frequency and stability. As one of the key elements in wireless networks, the local oscillator (LO) needs to operate at millimetre-wave (30GHz-300GHz) and THz (300GHz-10THz) band with lower phase noise, which becomes a major challenge for fifth generation (5G) wireless network and beyond. Thus, the OEO is greatly desired for LO in 5G wireless network and beyond.

The thesis introduces three OEO systems predicated on integrated devices designed to produce microwave signals characterized by high frequency, low phase noise, and tunability. The subsequent sections provide an in-depth elucidation of the primary content and innovations presented in the thesis. Three OEO schemes, leveraging photonic integrated circuit (PIC) technology, are posited to generate microwave signals featuring high frequency, low phase noise, and tunability.

The initial proposal involves a single-loop OEO utilizing a mode-locked laser (MLL) chip. The narrow-band gain spectrum of the MLL chip is harnessed to achieve stable oscillation in a single mode, resulting in the generation of a microwave signal with a

frequency tuning range of 23.91-24.71 GHz and an optimal phase noise of -80 dBc/Hz (@10 kHz). (Chapter 3)

Subsequently, a dual-loop OEO system is introduced, incorporating an extended feedback loop. To enhance phase noise and mitigate suppression ratio, a dual-loop coupled OEO employing the vernier effect is advanced. This configuration yields a tunable microwave signal with a frequency range from 23.68 GHz to 24.82 GHz, achieving a superior phase noise of -100 dBc/Hz (@10 kHz) and a side mode suppression ratio exceeding 40 dB. (Chapter 3)

In pursuit of further phase noise reduction and scheme simplification, an OEO based on parity-time symmetry is proposed, employing the MLL chip. This arrangement results in the generation of a tunable microwave signal within the range of 24–25 GHz, with a phase noise measuring below -108 dBc/Hz (@10 kHz). (Chapter 4)

This MPhil. project aims to propose integrated OEO with low power consumption and cost. This dissertation summarises the progress that has been made as far as so on and discusses the plan of further studies.

Impact Statement

This thesis focuses on optimising the performance of radio frequency (RF) signals generated by coupled optoelectronic oscillator (OEO). The generate high-performance RF signals that are highly needed in optical communication and radar systems. The key innovation of the studies is the ultra-low phase noise resulting from the high-quality-factor of the OEO cavity, which is achieved by using high-quality-factor optical energy storage elements, such as low-loss optical fiber or a high-quality-factor optical resonator.

In addition, the cost and power consumption of solutions using discrete OEO to generate high-frequency signals are relatively high. To realize a compact and low power-consumption OEO system, this thesis proposes a design method for a partially integrated coupled OEO. By employing a monolithic mode-locked laser (MLL) chip, microwaves of tunable frequencies from 23.68 GHz to 24.82 GHz are achieved at phase noise of approximately –100 dBc/Hz at 10 kHz offset. The robust design of this OEO system is advantageous for integration and thus exhibits potential for application in the miniaturization of microwave generation devices. Originating from the non-Hermitian quantum mechanics, the parity-time (PT) symmetry has been extensively explored to ensure a stable single-mode oscillation for OEOs, while avoiding additional extremely challenging ultrahigh-Q filters. Enabled by the emerging photonics integrated circuit (PIC) technology, this thesis reports the tunable PT-symmetric OEO by using an integrated mode-locked laser, as a striking advance to reduce the footprint of OEOs. Stable single-mode oscillating signal at 24.5 GHz has been generated with a phase noise of 108 dBc/Hz @ 10 kHz frequency offset. In particular, a tunable frequency range from 24 to 25 GHz is achieved by manipulating the injection currents into the well-designed on-chip linear laser cavity. This work exhibits a breakthrough in conceptual integrated microwave photonic devices, and also accelerates the real-world applications of fundamental physical theory of PT symmetry to information industry.

Moreover, this project investigates the recent developments of the OEO, and especially introduce the prospect of OEO serving as a qualified LO in the 5G wireless network and beyond. The OEO has better phase noise performance at high frequency, which is greatly desired for LO in 5G wireless network and beyond. Besides, the OEO provides an easy and low-loss method to distribute and synchronize mm-wave and THz LOs. Thanks to PIC development, the power consumption and cost of OEO reduce gradually. It is foreseeable that the integrated OEO with lower cost may have a promising prospect in the 5G wireless network and beyond.

Acknowledgements

I would like to extend my sincere appreciation to my supervisor, Prof. Huiyun Liu, for providing me with the invaluable opportunity to pursue my MPhil studies in this cutting-edge research field. Prof. Liu's dedication to the EEE department has left a lasting impression on me. He is not only a kind and supportive supervisor but also grants me significant freedom to explore areas of genuine interest. I am truly grateful for his unconditional trust and continuous encouragement throughout my study period.

I owe a debt of gratitude to Dr. Siming Chen and Dr. Zizheng Cao, from whom I acquired the majority of my knowledge in EEE growth. Dr. Cao, a brilliant researcher, consistently generates innovative ideas, and I am thankful for his patience and helpful guidance in reviewing my manuscripts. Special thanks also go to Dr. Fang Zou for his valuable advice on proper paper writing and for being an outstanding researcher.

I am fortunate to work with Dr. Mingchu Tang Dr.Ying Lu and Dr. Shujie Pan. Thank you all for being by my side, inspiring me and help me in London.

My heartfelt gratitude goes to my parents Mr. Xiaoxiao Zou and Mrs. Biying Zhang. I appreciate your unwavering support, continuous encouragement, and boundless love. You have always been my strongest backup, and I hope to have made you proud.

List of Publications

1. Fang Zou†, **Lei Zou**†, *et al*., “Optoelectronic oscillator for 5G wireless networks and beyond,” *J. Phys. D*, vol. 54, pp. 423002, 2021.

2. Fang Zou†, **Lei Zou**†, *et al*., “Parity-time symmetric optoelectronic oscillator based on an integrated mode-locked laser,” *J. Quantum Elect*., Vol. 57, pp. 500209, 2021.

3. Fang Zou†, **Lei Zou**†, *et al*., “Reciprocal Phase Transition Electro-Optic Modulation**,”** *Laser Photonics Rev*. Vol. 17, pp. 2200577, 2023.

   († contributed equally)

Contents

LIST OF ABBREVIATIONS

OEO	Optoelectronic oscillator
LC	Inductance-capacitance
COEO	Coupled optoelectronic oscillator
IOEO	Integrated optoelectronic oscillator
RF	Radio frequency
PD	Photodetector
EOM	Electro-optical modulator
LNA	Low noise amplifier
ESA	Electrical spectrum analyser
DC	Direct current
WGMR	Whispering gallery mode resonator
SMF	Single-mode fiber
YAG	Yttrium Aluminum Garnet
MZM	Mach-Zehnder modulator
EBPF	Electrical band-pass filter
VCP	Voltage-controlled phase shifter
SOA	Semiconductor optical amplifier
MLL	Mode-locked laser

IMWP	Integrated microwave photonics
SOI	Silicon on Insulator
InP	Indium Phosphide
Si_3N_4	Silicon Nitride
MDR	Micro-disk resonator
DFB	Distributed feedback
DBR	Distributed Bragg reflector
PM	Phase modulator
DML	Directly modulated laser
PolM	Polarization modulator
PC	Polarization controller
EF	Electrical filter
EDFA	Erbium doped fiber amplifier
EA	Electrical amplifier
PS	Phase shifter
OF	Optical filter
TLS	Tunable laser source
OSA	Optical spectrum analyser
VNA	Network analyser

FWHM	Full width at half-maximum
MIR	Multimode reflector
SA	Saturable absorber
OFC	Optical frequency comb
EAM	Electrical absorption modulator
PBS	Polarization beam splitter
PT	Parity-Time
BPD	Balanced photodetector
TDL	Time delay line
FSR	Frequency space range
5G NR	Fifth-generation new radio
3GPP	Third-generation partnership project
LO	Local oscillator
EIC	Electronic integrated circuit
MIMO	Multiple input multiple output
PLL	Phase-locked-loop laser
SNR	Signal-to-noise ratio
EVM	Error vector magnitude
BW	Broader bandwidth

QPSK	Quadrature phase shift keying
QAM	Quadrature amplitude modulator
ADC	Analog-to-Digital Converter
PIC	Photonics integrated circuit
MPW	Multi project wafer
BBU	baseband unit
RRUs	remote radio units
BS	Base station
CMOS	Complementary Metal-Oxide-Semiconductor
ANs	Access nodes
C-RAN	Co-operative Radio Access Network

List of Chemical Elements

Si	Silicon
In	Indium
P	Phosphorus

List of Symbols

Q	High-quality-factor
τ_d	Loop-decay time
f	Resonator frequency
Δf	Frequency spacing
n	Fiber optic effective refractive index
c	Speed of light
L	Length of the loop delay line
ϕ	Phase
ω	Angular frequency
α	Amplitude
v	Voltage
t	Time scale
I	Photocurrent
R	Resistor
G_A	Amplified coefficient
V_π	Half-wave voltage
η	Extinction ratio of the modulator
f_k	Offset frequency

f_c	Carrier frequency
f_0	Central frequency
Γ	Full width at half-maximum
P_{osc}	Carrier power
f_s	Frequency shift
θ	Phase jitter

List of Figures

List of Tables

Chapter 1. Introduction

1.1. Preface

By combining microwave and photonic technologies, optical devices are employed to generate, transmit, process, and measure microwave signals. This convergence has given rise to an emerging interdisciplinary discipline known as microwave photonics [1]. Thanks to photonic technology, the advantages of large bandwidth, low loss, and resistance to electromagnetic interference, combined with mature and highly efficient microwave technology, provide excellent resolution and easy control. These advantages effectively complement each other in microwave photonic systems, resulting in enhanced performance and capabilities. Particularly in the current 'data' era, microwave photonic technology has found extensive applications in broadband radars, wireless communications, and mobile technologies [4]. Numerous research breakthroughs have been achieved in both national defence and civilian applications, including areas such as remote sensing and ubiquitous connectivity. For example, microwave photonics technology has enabled high-frequency, high-quality microwave signal generation, arbitrary waveform generation, high-capacity communication transmission systems, multi-node acquisition systems, and broadband signal processing, among other applications. In microwave photonics, the primary applications involve the generation of high-frequency, high-quality microwave signals through techniques such as heterodyne and Opto-Electronic Oscillator (OEO) [9]. The OEO achieves a notable reduction in phase noise due to the high-quality factor (Q-value) associated with prolonged fiber length. Importantly, this phase noise is independent of oscillating frequency. Consequently, the OEO is adept at satisfying the requisite phase noise specifications when employed as a Local Oscillator (LO) in advanced communication networks, including the 5G wireless network and

subsequent technological iterations. However, discrete devices used in microwave photonic system may not excel in terms of system size, power consumption, and stability. Therefore, a significant research focus lies in adopting integrated microwave photonic chips for microwave signal generation, addressing these concerns and advancing the field [11]. Within this chapter, an extensive review of the OEO technology is undertaken, practical applications, and noteworthy milestones in its representative implementations.

1.2. Optoelectronic oscillator

1.2.1. Oscillators

Repetitive variation around a central point or between two states in a time --- this phenomenon is called oscillation. Oscillations exist in various occasion such as human heart, business cycle and so on [12]. The oscillation that occurred from oscillators is most widely used in our society from the past to now. For instance, a spring-mass and a clock pendulum are traditional mechanical oscillators. Two of the typical oscillators are Var den Pol and OEO in the engineering field. Both can be used to generate a microwave signal with low phase noise. It is required in various applications such as metrology, communications and radar systems. Based on the electronic and optical domain, oscillators create periodic waves by converting direct current from a power supply. These periodic waves' amplitude, phase and frequency can be precisely controlled to generate signals that carry information [13].

The electronic oscillator was initially proposed by supplying an inductance-capacitance (LC) tuned circuit in parallel with an electric arc and a magnetic blowout in 1892 [17]. Figure 1.1 shows a typical LC Electronic Oscillator. Then, the Hartley oscillator, known as the first LC oscillator whose oscillating frequency is determined by a tuned circuit consisting of capacitors and inductors, was invented and led to the

dramatic development of oscillating electronic technology in centuries [18]. With the rapid development of information society, the signals of high performance such as high-frequency band, low phase noise, pure spectral and frequency stability are urged to apply in diverse fields of science ranging from sensing, radar and communications. However, those electronic oscillators have limits on those performance and other aspects like bulky, high-power consumption and high price. For instance, the researchers pursue an energy storage element with the high-quality value (high-Q) and the ultra-low transmitted loss to realize the pure and stable spectrum when exploring the electronic oscillator. However, it is hard to configure a high-Q value in the electronic oscillator because the intrinsic loss would deteriorate the performance of power communication. Hence, researchers introduce OEO to improve the performance [21]. The OEO is an oscillator that converts the continuous light energy to microwave signal. Notable that, the OEO is based on using high-Q optical waveguides and resonators so that the loss is much lower than the electronic counterparts. Thanks for ultra-low loss of fibre and large bandwidth of microwave photonic system, the OEO system has been wildly implemented to generate microwave signal with high frequency and ultra-low phase noise [22].

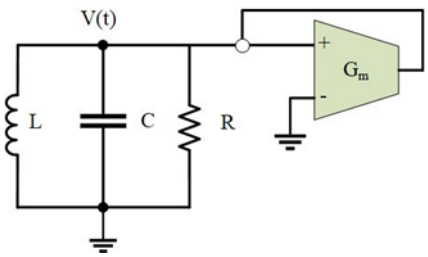

Figure 1.1 Configuration of LC Electronic Oscillator.

1.2.2. Basic Scheme of Optoelectronic oscillator

Typically, an OEO system consists of a tunable laser source, an electro-optical modulator (EOM), and an optical delay line, a photodetector (PD), an electrical

amplifier (EA), and an Electrical band-pass filter (EBPF), as show in Figure 2.1. A Lithium Niobate Mach-Zehnder modulator (MZM) usually serves as the EOM and a single-mode fiber (SMF) serves as the optical delay line. The light emitted from a tunable laser source is transmitted through the SMF after modulated by the MZM. Then, the modulated light is detected at the PD, where the light converts to an RF signal by the optical envelope detection. In the Radio frequency (RF) part, an EA and an EBPF are necessary for providing enough gain and selecting the oscillating mode. Only the loop gain exceeds the total loss at a certain frequency while its phase increases 2π in each circulation, could the selected mode steadily oscillate. Under these criteria, OEO generates a RF signal with high frequency and ultra-low phase noise [23].

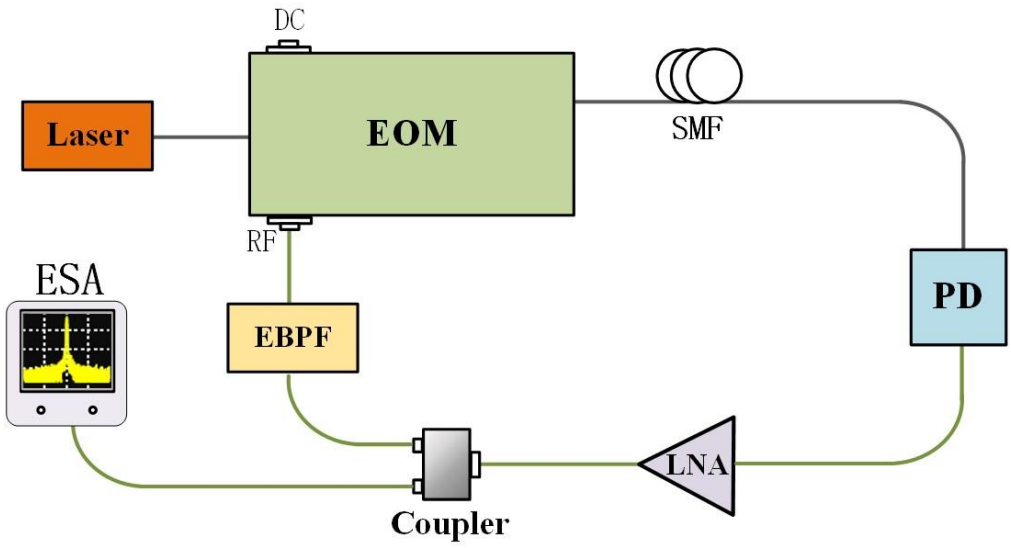

Figure 1.2 Generic configuration of OEO. (OEO: Optoelectronic Oscillator. EOM: Electro-optical modulator. SMF: Single-mode fiber. PD: Photodetector. LNA: Low noise amplifier. EBPF: Electrical band-pass filter. DC: Direct current. RF: Radio frequency. ESA: Electrical spectrum analyser.)

1.2.3. Major parameters of Optoelectronic Oscillator

Quality (Q) factor: The Q factor is the ratio of the peak energy stored in the resonator in a cycle of oscillation to the energy lost per unit of the cycle, which is given by:

$$Q = 2\pi f \tau_d \qquad \text{(eq.1)}$$

Where τ_d is the loop-decay time, which measures the energy-storage capability of the resonator, f is the resonator frequency [24].

Phase noise: Phase noise is a measure of the short-term stability of an oscillator. It quantifies the random variations in the phase of the output signal over time. Phase noise is typically specified in terms of its power spectral density, which describes how the noise power is distributed across different frequency components [25]. In our project, Phase noise is defined as the ratio of the noise power in a 1 Hz bandwidth at a certain frequency offset to the signal power at the central frequency, which is measured in dBc/Hz. Notable that the phase noise is directly influenced by quality storage elements, and this principle will be demonstrated in Chapter 2 in detail.

Frequency tunability: Frequency tunability refers to the capability of a system, device, or component to adjust or vary its operating frequency. In the context of electronic or optical systems, frequency tunability allows the user to change the output frequency within a specified range. This feature is particularly important in various applications where the frequency of a signal needs to be adjusted to meet specific requirements or adapt to different operating conditions. Frequency tunability is crucial in various applications such as wireless communication, radar systems, spectroscopy, and signal processing, where the ability to adapt to different frequency requirements is essential for optimal performance [27].

1.3. Optoelectronic Oscillator for microwave generation

1.3.1. Optoelectronic Oscillator based on discrete device.

Significantly, the optical cavity can be any type of resonator such as optical fiber or whispering gallery mode resonator (WGMR). Thanks to the flexible configuration, the OEOs can act as crucial devices in various applications including generation, sensing,

and detection [28]. Particularly, the feature of the ultra-low phase noise makes OEO suitable for LOs for radars and communication systems. In the subsequent discourse, certain fundamental architectures of OEO employed in the generation of RF signals. These architectures encompass the single-loop OEO, the multi-loop OEO, the coupled OEO, and the tunable OEO.

1.3.1.1. Single-loop Optoelectronic Oscillator

To improve the performance of the generated microwave signal, a high-Q storage element is introduced into the optoelectrical feedback loop, such as SMF. By placing a long fiber as the optical cavity to obtain high-quality, this kind of configuration of OEO can achieve an ultra-low phase noise [29]. In Figure 1.3, the L. Maleki team produces a single-loop OEO consisting of an Yttrium Aluminum Garnet (YAG) laser, a MZM, a 16-km long fiber and low noise electrical devices. Besides, a thermal stabilized box covers the long fiber to reduce frequency drift caused by environmental factors. The phase noise of generated signal (10GHz) is low to -163 dBc/Hz at 6kHz offset frequency [30].

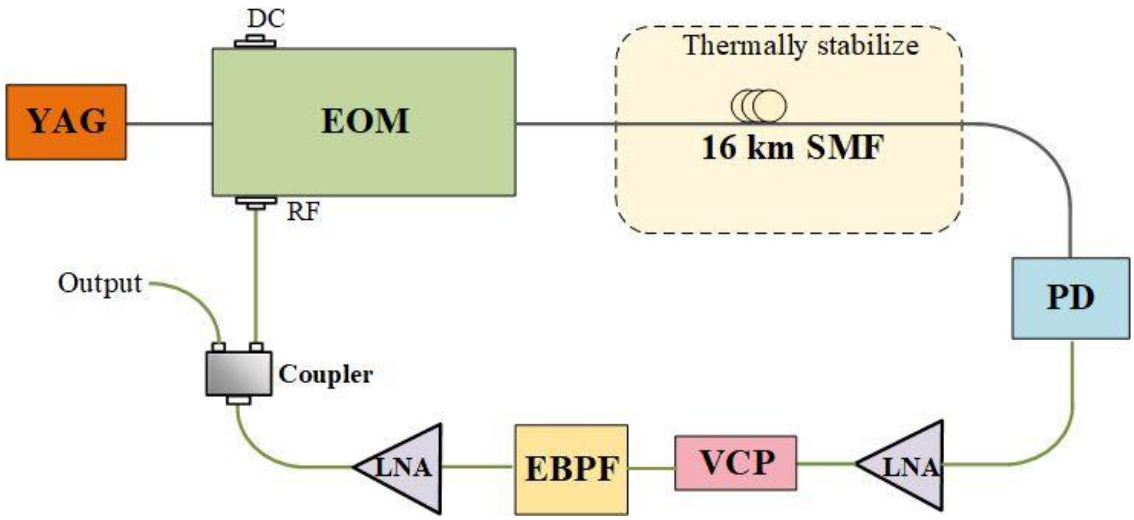

Figure 1.3 Configuration of single-loop OEO. (YAG: Yttrium Aluminum Garnet laser. SMF: Single-mode fiber. VCP: Voltage-controlled phase shifter. EOM: Electro-optical modulator. SMF: Single-mode fiber. PD: Photodetector. LNA: Low noise amplifier. EBPF: Electrical band-pass filter. DC: Direct current.)

1.3.1.2. Multi-loop Optoelectronic Oscillator

As mentioned in the last section, a long fiber can be supplied as an energy storage element in OEO to achieve high performance. However, the oscillating mode space is reciprocal of the length of the optical cavity [30].

$$\tau_d = \frac{1}{\Delta f} = \frac{nL}{c} \qquad \text{(eq.2)}$$

Where Δf is the frequency spacing, n is the fiber optic effective refractive index, c is the speed of light and L is the length of the loop delay line. From equation (eq.2), the longer the loop delay results in the smaller the frequency spacing. In contrast, the small frequency spacing may cause mode hopping problems and difficulty realizing the ability of mode selection. For instance, when a 16 km length single-mode fiber is implemented in the scheme, the mode space decreases to a range of tens of kilohertz. Thus, a mode-selection mechanism is required for the oscillating system. Traditionally, an EBPF is the first choice. However, this limits tunability because of its fixed central frequency. To solve this problem, multi-loop OEO with deferent loop length is proposed.

In this scheme, the longer loop determines the phase noise of OEOs, whereas the shorter loop determines the mode space [32]. When some of the modes generated by each loop are oscillating in phase, a stable oscillation can be achieved with an oscillating frequency that satisfies:

$$f_{osc} = \frac{k}{\tau_1} = \frac{m}{\tau_2} \quad \text{(eq.3)}$$

Where k and m are integers; τ_1 and τ_2 are time delays in each loop. This method, known as the Vernier effect, can both realize high Q and mode selection. Figure 1.4 is the scheme of multi-loop OEO. By supplying a dual-loop delay line, the mode space can be enlarged. Even more to the point, an EBPF in this scheme is to suppress the side modes to reduce the spurious levels. However, the overall Q is determined by the Q-value, which is an average figure of long loop and shot loop. The phase noise is slightly smaller than the single-loop OEO.

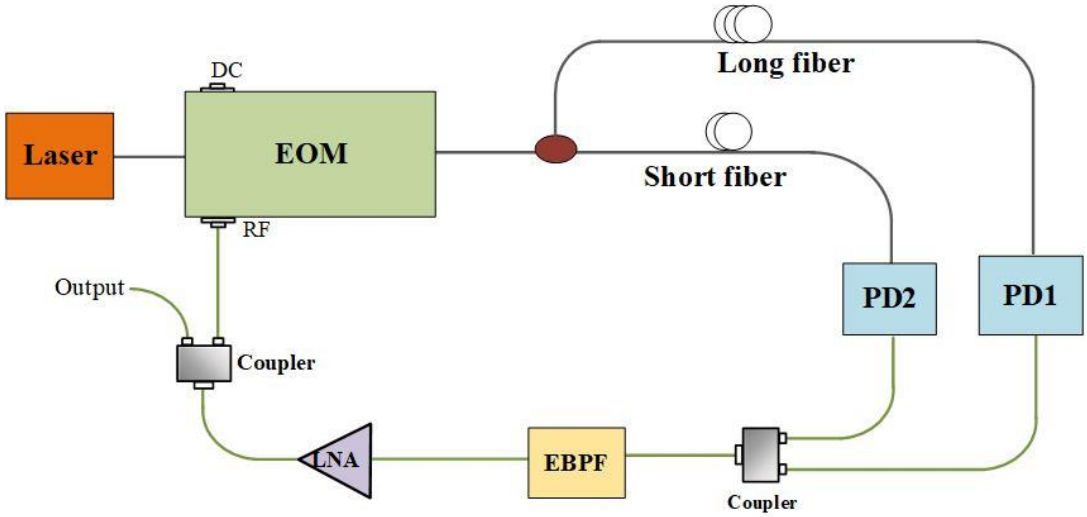

Figure 1.4 Configuration of Dual-loop OEO. (EOM: Electro-optical modulator. PD: Photodetector. LNA: Low noise amplifier. EBPF: Electrical band-pass filter. DC: Direct current.)

1.3.1.3. Injection-locked Optoelectronic Oscillator

The injection-locked OEO(IL-OEO) was invented to solve multi-loop OEO limitations [33]. A typical scheme of IL-OEO can be seen in Figure 1.5. There are two different lengths single-loop OEO injection-locked as one OEO. The long-loop OEO is master OEO and the short one is called slave OEO. When the signal frequency from slave OEO is close to the frequency of master OEO, and injected enough power, the spurious level can be reduced according to the frequency pulling effect. This configuration can realize low phase noise and spectral purity. The dual-loop IL-OEO can generate a 10GHz signal with -134 dBc/Hz phase noise at the offset frequency of 10kHz [34].

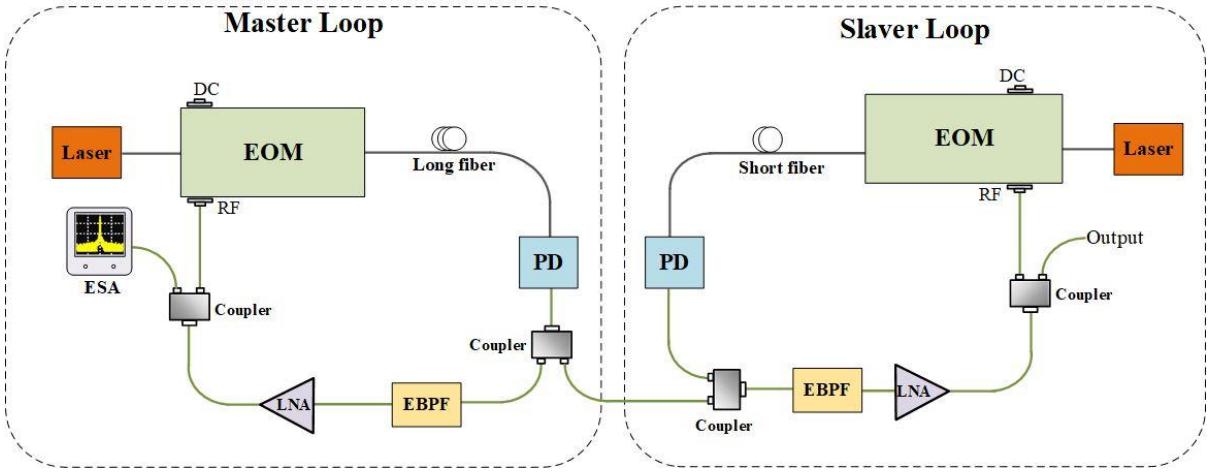

Figure 1.5 Configuration of Injection-locked OEO. (EOM: Electro-optical modulator. PD: Photodetector. LNA: Low noise amplifier. EBPF: Electrical band-pass filter. DC: Direct current. ESA: Electrical spectrum analyser.)

1.3.1.4. Coupled Optoelectronic Oscillator

Although the IL-OEO can realize high performance, the scheme is bulky and has large power consumption. The laser oscillation is directly coupled with the electronic oscillation in the OEO configuration is named coupled OEO (COEO). The COEO structure includes a positive optical feedback loop around the high-Q element, and the Q enhancement is multiple the quality factor of the passive storage element. Thus, it realizes high performance as well as a compact configuration [35]. The D. Eliyahu's team proposed a COEO structure that is compact also obtain a low phase noise RF [30]. Figure 1.6 shows a typical COEO scheme that supplies an optical feedback loop as energy storage to get a high-Q. The deferent sections with other OEO configurations are that the light source consists of a semiconductor optical amplifier (SOA) and MZM instead of a traditional laser. Secondly, the generated signal is amplified and filtered by the Low noise amplifier (LNA) and EBPF then fed back to MZM. Lastly, the fiber in COEO is only 140 meters. Thus, the spur of the microwave signal generated by COEO is easily blocked by the filter and obtains a low phase noise of -148dBc/Hz at 10kHz offset frequency. Notably, the COEO can imply a frequency

comb (OFC) area because this scheme can act as a mode-locked laser to generate an optical train in the time domain [36].

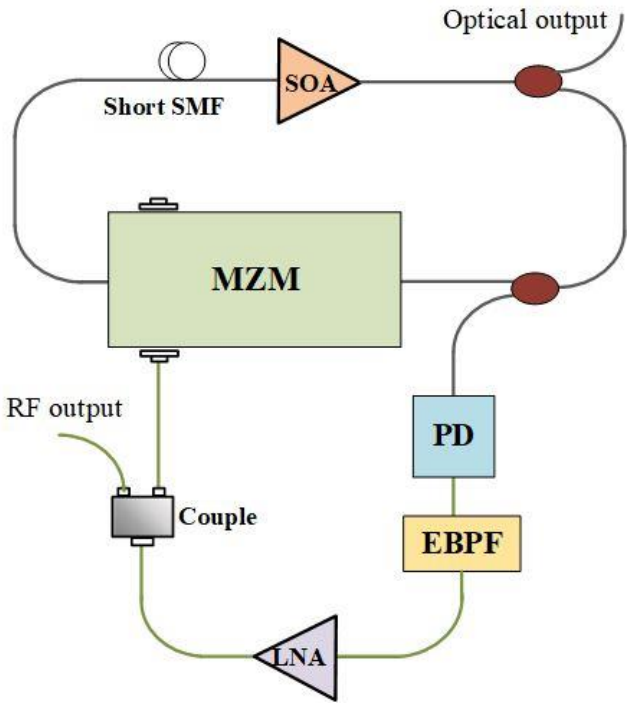

Figure 1.6 Configuration of Coupled OEO. (MZM: Mach-Zehnder modulator. SMF: Single-mode fiber. PD: Photodetector. LNA: Low noise amplifier. EBPF: Electrical band-pass filter. RF: Radio frequency. SOA: Semiconductor optical amplifier.)

1.3.1.5. Performances of discrete Optoelectronic Oscillator system

In summary, OEO generates spectrally pure microwave signals in the high-frequency band. In order to achieve the spurious suppression of side modes and maintain the high-Q factor of the OEO loop, the multi-loop OEOs, the injection-locked OEOs and the coupled OEOs have been proposed [37][53]. Furthermore, OEO architectures based on optical or microwave photonics filter have been developed to enable wideband tunable microwave signal generation. To clear the development of the OEO for microwave signal generation, the OEO applications and their performances have been summarized in Table 1.

Table 1 Review for discrete OEO

Scheme	Freq. (GHz)	P.N. @10kHz (dBc/Hz)	Year	Ref.
Single loop OEO	9.56	-130	1996	[21]
Multi-loop OEO	10	-140	1998	[32]
COEO	18.2	-85	2000	[36]
Single loop OEO	10	-163 (@6 kHz)	2008	[30]
Multi-loop OEO	DC-60	-100	2015	[40]
COEO	10	-117	2017	[41]
Tunable OEO	8.6-15.2	-110.88	2018	[44]
Sigle-loop OEO	12-20	-114	2019	[42]
Phase-locked OEO	8-12GHz	-139	2019	[43]
Injection-locked OEO	8-12GHz	-138	2019	[52]
Multi-loop OEO	10	-117.6	2020	[45]
Injection-locked OEO	94.5	-101	2020	[46]

Freq. frequency, P.N. phase noise, Tech. technology, Ref. reference, Pow. power, DC. Direct Current.

The microwave signal whose frequency exceeds 90 GHz, or phase noise is -163 dBc/Hz @ 6-kHz offset frequency, or tunable range is from direct current to 60 GHz can be realized by using different OEO architectures. More importantly, the OEO system seems to be a potential solution for distributing and synchronizing RF signal with low transmitted loss in the 5G wireless network and beyond. However, these OEOs based on discrete components are too bulky to implement in the real industry. To meet the requirements of practical applications, such as compact size and low driven power, integrated OEOs come into the insight of the researchers.

1.3.2. Integrated Optoelectronic Oscillator

As aforementioned, the OEOs achieve remarkable development in the past tens of years. However, the bottlenecks of bulk size and power consumption hinder the popularization and industrialization of OEO. Hence, the development of photonics

integrated circuit (PIC) has made OEO technology to meet the requirements of practical applications, compact size, and low driven power [54][67]. Some important integrated OEOs and their performances are reviewed in this section.

1.3.2.1. Partially integrated Optoelectronic Oscillator

Firstly, some partially integrated OEO architectures are reported on different PIC platforms [54]. In [54], a silicon-on-insulator (SOI) chip including a high-speed phase modulator, a thermally tunable micro-disk resonator (MDR), and a high-speed PD is fabricated, and the integrated OEO is implemented to generate a tunable microwave signal, as shown in Figure 1.7(a). Based on the phase-modulation to intensity-modulation conversion, a frequency tuning range of 8 GHz is realized, and the phase noise is lower than -120 dBc/Hz at 1 MHz offset frequency. In addition to the SOI chip, the indium-phosphide (InP) platform is widely used to fabricate active devices, especially laser sources, because InP materials have a direct bandgap. In [55], an integrated OEO with a tuning range from 15 to 20 GHz is generated by integrating two distributed feedback (DFB) lasers on an InP chip, as shown in Figure 1.7 (b). With the cross-injection and OEO technology, the phase noise is -95 dBc/Hz at 100-kHz offset frequency. Moreover, to avoid the RF loss caused by external EOM in conventional OEO systems, an integrated OEO by using the optical injection of a directly modulated laser was demonstrated. In [56], X. Zhang et al. proposed an OEO based on an integrated multi-section DFB laser, as shown in Figure 1.7(c). Such compact OEO generates a 20.3-GHz microwave signal with a phase noise of -115.3 dBc/Hz at 10-kHz offset frequency. Recently, a parity-time symmetric OEO based on an integrated mode-locked laser is reported as a breakthrough for developing next generation OEOs [57].

Figure 1.7 The key devices of partially integrated OEO system. (a) OEO based on a chip [54]. (b) OEO based on two DFB lasers integrating on an InP chip [55]. (c) OEO based on an integrated multi-section DFB laser. [56] (SOI: Silicon on Insulator. InP: Indium Phosphide. DFB: Distributed feedback.)

1.3.2.2. Compact Optoelectronic Oscillator module

However, the partially integrated OEOs still use some discrete optical and electrical components. It is hard to further reduce the footprint and cost to meet the requirements of industrialization.

Figure 1.8 The chip of the compact OEOs. (a) A compact OEO integrated on an InP substrate[58]. (b) The OEO chip based on a lithium-niobate WGMR [59]. (InP: Indium Phosphide. WGMR: Whispering gallery mode resonator.)

Thus, a lot of efforts were devoted to high-performance microwave oscillators that are not only of miniature size but also have low power consumption. Typically, some compact OEOs are reported in recent years [37][39]. The optical parts of the compact OEOs are integrated and packaged with electrical parts into a miniature module. In [58], J. Tang demonstrated a compact OEO that the optical parts are monolithically integrated on an InP substrate. And the optical and electrical parts are packaged on a print circuit board with the size of 5*6cm^2, as shown in Figure 1.8(a). The oscillating frequencies are 7.30 and 8.87 GHz in different injected currents, and phase noises are -92 dBc/Hz and -93 dBc/Hz at 1-MHz offset frequency, respectively. In [22], an OEO chip based on a lithium-niobate whispering gallery mode resonator (WGMR) has been released by the OEwave company, which is the first commercially used compact OEO module, as shown in Figure 1.8(b). It generates a 30 GHz (or higher) microwave signal with a phase noise of -108 dBc/Hz at 10-kHz offset frequency. The size of the OEO chip is 19.35 mm^2 and the power consumption is 2.5 W. As a major milestone

for OEO, this work exhibits a breakthrough in OEO for microwave generation, and also speeds up real-world applications of OEO [59].

Table 2 Review for integrated OEO

Partially integrated OEO					
Tech.	**Freq. (GHz)**	**P.N. @ 10 kHz (dBc/Hz)**		**Year**	**Ref.**
WGMR	8-40	-120		2010	[65]
MLL on InP	20	-110 (@ 10MHz)		2013	[61]
Disk resonator on a SOI	21.7	-90		2013	[62]
Dual-mode laser on InP	37.5-43.59	-94.87		2017	[63]
DML on InP	2.2-19.5	-110		2018	[66]
Multi-section DFB on InP	20.3	-115.3		2019	[56]
MLL on InP	24-25	-108		2021	[57]
Compact OEO module					
Scheme	**Freq. (GHz)**	**P.N. @ 10kHz (dBc/Hz)**	**size**	**Pow. (W)**	**Year**	**Ref.**
DML	8.87	-92(@ 1MHz)	5*6 cm^2	-	2018	[58]
WGMR	28-36	-110	0.06 in^3	2.5	2010	[59]

Freq. frequency, P.N. phase noise, Tech. technology, Ref. reference, Pow. power.

1.4. Local oscillator

LO often serves as a reference for the carrier signal to up-convert and down-convert the output and incoming data, respectively. When the radio signal with data is received and demodulated, recovering and synchronizing the carrier are always required. The LO should be a clean and stable source so that the transceiver can well synchronize and recognize the carrier. The phase noise of the LO should be low enough to ensure a good signal-to-noise ratio (SNR). As the LO is indispensable in the transceiver, improving the performances of LO is an important research topic in the 5G and beyond wireless network. For example, the phase noise of the LO is a random fluctuation causing detection error of the received signal spectrum. Also, the phase noise of LO destroys the orthogonality of the subcarriers in orthogonal frequency division multiplexing (OFDM) systems and degrades the performance by producing intercarrier interference [68][74].

To support more complex services in 5G and beyond, the broader bandwidth (BW) and more efficient modulated formats are necessary [75][79]. Hence, LOs with high frequency and outstanding performances are crucial for the 5G and beyond wireless network. Some new requirements on the LO for 5G and beyond are summarized in the following.

Firstly, an ultra-stable LO in the frequency band of millimetre-wave (30GHz-300GHz) or THz (300GHz-10THz) is required. The frequency error in the transceivers is mainly attributed to the frequency accuracy of the LOs, and the environment factors (e.g. temperature) may also deviate the carrier frequencies. Besides, the higher carrier frequency poses challenges in synchronizing the synchronized carrier components (CCs) and recovering the baseband signal since mm-wave and THz band exhibit more

loss and nonlinearity. To solve these problems, a more accurate and stable oscillator with a high frequency is necessary.

Secondly, high-order modulated formats such as 128/256 quadrature amplitude modulator (QAM) can improve the spectrum efficiency and realize an ultra-high bit rate [78]. To realize the complex modulated formats, the SNR and the error vector measurements (EVM) are critical in the transceiver. For simplicity, the EVM is an integration of phase noise beyond tracking BW and inside channel (broader bandwidth) BW. Therefore, the phase noise of the LO affects the performance of the transceiver directly.

Thirdly, small cells which is cover unit of cellular wireless networks will also play an important role in 5G and beyond wireless network since the small cells are used to reduce loss of the wireless link and increase data rates. When using small-cell architecture and massive multiple input multiple output (MIMO) technology, a large number of LOs are needed in the wireless network with the increasing of the transceiver. From the perspective of the frequency synchronization and the cost reduction, generating synchronized carrier components (CCs) in a central baseband unit (BBU) pool and distributing it to remote radio units (RRUs) may arise as a feasible option [79].

1.5. Objectives and Outline

The aim of the MPhil. project is to invent an integrated OEO based on high-performance RF generation. The principal objectives of this MPhil. project is:

1. To demonstrate the different types of OEO.
2. To demonstrate the performance evaluation of OEO.
3. To demonstrate the integrated OEO.

The first chapter of this report discusses the motivation literature review on research activities, followed by introducing the experimental instruments in Chapter 2. The up-to-date progress is illustrated in Chapter 3 and 4, including the single-loop OEO, dual-loop coupled OEO and Parity-time Symmetric OEO proposal. A future research plan is made in Chapter 5.

Chapter 2. Methodology

In the research, the system of Optoelectronic oscillator (OEO) has been modelled by MATLAB as well as the simulation result. The experiment setup is introduced in the following parts. In order to evaluate the performance of RF microwave generated by OEO, the electrical spectrum analyser (ESA), optical spectrum analyser (OSA) and vector network analyser (VNA) has been used.

2.1. Theoretical model

2.1.1. Model for Optoelectronic oscillator

The first theoretical model of the OEO was proposed by X. S. Yao and L. Maleki in 1996 [80]. Based on the quasi-linear theory, the overall relationship between the output of the amplifier and the input of the electro-optical modulator (EOM) is analysed. By using the regenerative-feedback approach, this model analyses the final steady-state spectra of OEO after thousands of oscillations. Furthermore, Levy et. al., introduce a slow variation on the amplitude envelope to analyse the dynamical effects from the start-up to the stable oscillation. Thus, a new and comprehensive model is proposed for single-loop OEO [81]. Beyond the physical effects in the Yao-Maleki model, this model as well as includes some dynamical effects of OEO, such as the fast response time of the modulator, the ability of the OEO to oscillate in several modes and signal fluctuations induced by the input noise. Except for the quasi-linear theory, Chembo et. al., proposed a nonlinear dynamic approach to study the signal dynamics in OEO [82]. Using the delay-differential equation (DDE), the model could analyse the interaction between the delay and the intrinsic nonlinearity resulting in unsuspected bifurcation-induced instability. However, this model assumes that the mode space is smaller than

the bandwidth of the filter and signal variation is small. In other words, it is not a general model for the OEO system.

A system simulation program has been made for single-loop OEO signal generation by MATLAB, which referred to Levy's OEO model. The schematic of the OEO is shown in Figure 2.1. To analyze the relationship between the input signal of the EOM and the output of the electrical amplifier (EA), assuming the input signal is $V_{in}(t,T)$ and the output signal is $V_{out}(t,T)$. Because the quality factor of the EBPF is extremely high, the $V_{in}(t,T)$ can be approximated as a sinusoidal wave with an angular frequency ω_c, a time dependent phase $\phi(T)$ and a time dependent amplitude $\left|\alpha_{in}^{\mathrm{mod}}(T)\right|$. It can express as:

$$\begin{aligned} V_{in}(t,T) &= \left|\alpha_{in}^{\mathrm{mod}}(T)\right|\cos[\omega_c t+\phi(T)] \\ &= \frac{1}{2}\alpha_{in}^{\mathrm{mod}}(T)\exp(-i\omega_c t)+c.c. \end{aligned} \qquad \text{(eq.4)}$$

Where $\alpha_{in}^{\mathrm{mod}}(T)=\left|\alpha_{in}^{\mathrm{mod}}(T)\right|\exp[-i\phi(t)]$ is the complex envelope of the input $V_{in}(t,T)$. It is noticed that the expression of the input voltage includes two kinds of the time scale. Specifically, a slow time scale *T* is determined by the roundtrip time (1-10 μs) and a fast time scale *t* is order of the periods of sinusoidal wave (10-100 ps). In addition, there is another time scale to describe the optical signal, but it can be ignored in this model. The output optical signal is determined by the $V_{in}(t,T)$ according to the nonlinear response of the EOM. Then the optical signal is converted to an RF signal and amplified to output electrical signal $V_{out}(t,T)$, which can be written as:

$$V_{out}(t,T)=V_{ph}(1-\eta\sin\{\pi[V_{in}(t,T)/V_{\pi}+V_B/V_{\pi}\}) \qquad \text{(eq.5)}$$

Where $V_{ph} = I_{ph} R G_A$ is the photodetector voltage, $I_{ph} = \rho \alpha P_0 / 2$ is the detected photocurrents at the Photodetector (PD), R is resistor, G_A is the amplified coefficient. V_π and V_B is the half-wave voltage and the Direct current (DC) bias voltage of the modulator. η is defined as the extinction ratio of the modulator, $(1+\eta)/(1-\eta)$. Combining the equations (eq.4) and (eq.5), it uses the Jacobi-Anger expansion to describe their relationship:

$$\begin{aligned} V_{out}(t,T) &= D.C. + H.H. + c.c. \\ &-\eta V_{ph} J_1(\pi \left|\alpha_{in}^{\mathrm{mod}}(T)\right| / V_\pi) \exp[-i\omega_c t + i\phi(T)] \end{aligned} \quad \text{(eq.6)}$$

Where J_1 is the first order of Bessel's function. Because the high-order harmonics (H.H.) and the D.C. are blocked by the Electrical band-pass filter (EBPF) and DC-block of PD, it may neglect them by using the quasi-linear theory when rejected back to the Mach-Zehnder modulator (MZM), while the nonlinear effects of high-order modes on the amplifier saturation is similarly neglected due to the quasi-linear theory.

Using quasi-linear theory approximation, only the first-order mode at the carrier angular frequency of ω_c would propagate within the cavity. Hence, the complex envelop of the EA output voltage can be written as:

$$\alpha_{out}^{amp}(T) = -2\eta V_{ph} J_1(\pi \left|\alpha_{in}^{\mathrm{mod}}(T)\right| / V_\pi) \exp[i\phi(T)] \quad \text{(eq.7)}$$

It is clear that the amplitude $\alpha(T)$ and phase $\phi(T)$ are variable on a slow time scale. Assuming the response EBPF is Lorentzian shape. After the EBPF, the filter output $\alpha_{out}^{fil}(T)$ can be described by the Fourier coefficient of filter input $\tilde{\alpha}_{in}^{fil}(f_k)$ and filter impulse response $F(f_k + f_c)$,

$$\begin{aligned}\alpha_{out}^{fil}(T) &= IFFT(\tilde{\alpha}_{out}^{fil}(f_k)) \\ &= IFFT(\tilde{\alpha}_{in}^{fil}(f_k) * F(f_k + f_c)) \\ &= IFFT(\tilde{\alpha}_{in}^{fil}(f_k) * \frac{i\Gamma/2}{f_k + f_c - f_0 - i\Gamma/2})\end{aligned} \quad \text{(eq.8)}$$

Where is the Fourier transform of $\alpha_{out}^{amp}(T)$, f_k is the offset frequency with respect of the chosen carrier frequency f_c, f_0 is the central frequency of the filter and Γ is the full width at half-maximum (FWHM) of filter transmission spectrum.

The complex amplitude of the signal inside the OEO on a round trip is calculated, then it would be iterated thousands of times to simulate the oscillation. The complex amplitude $\alpha^l(T)$ is defined as the interval of $\alpha_{in}^{fil}(T)$ in $(l-1)\tau \le T < l\tau$, where the l is the number of round trips and $\tau = n_{eff}L/c$ is the round-trip time of the OEO cavity. The next round trip $\alpha^{l+1}(T)$ is equal to the valid convolution between the amplitudes of the former adjacent two round trips and the filter impulse response. Then, the complex amplitude is fed back to the modulator, and calculate the response of EOM and PD within the next round trip. The noises including the thermal noise of amplifier, the shot noise of PD and the intensity noise of laser are added in the input of amplifier. It can approximate the total noises in the OEO as a white Gaussian noise with a single-sideband power spectral density of ρ_n.

After thousands of iterations $T_0 = N\tau$, it can get a steady-state oscillation. To analyse the performance of the OEO system, $\alpha_{M\tau}(T)$ is defined as the voltage amplitude for the time range from T_0 to $T_0 + M\tau$ and its discrete Fourier transform can be written as

$$\tilde{\alpha}_{M\tau}(f) = F_{M\tau}[\alpha(T)] = \frac{1}{M\tau}\int_0^{M\tau} \alpha_{M\tau}(T + T_0)\exp(2\pi i f T)dT \quad \text{(eq.9)}$$

In the theoretical model, the Radio frequency (RF) spectrum is approximately equal to the phase noise spectrum over a wide frequency range in OEO since the amplitude

noise is negligible and the phase fluctuation is much smaller than unit [74]. This approximation had been demonstrated in the theoretical simulation and experiment demonstration in former research. It can evaluate the performance of phase noise in the model by:

$$S_{\phi}^{M\tau}(f) \cong S_{RF}^{M\tau}(f) = \frac{\left|F_{M\tau}[\alpha(T)]\right|^2}{2RP_{osc}\delta f} \quad \text{(eq.10)}$$

Where $P_{osc} = \left|\tilde{a}(f=0)\right|^2 / 2R$ is the carrier power.

2.2. Simulation Result of modelling of single-loop OEO

In the simulation, the length of loop is assumed as L=10 m, 100 m, 500 m, 1000 m. As discussed in section 1, the more extended fiber line causes frequency space to be small. Thus, it needs an EBFP to suppress the unwanted modes. The bandwidth should be set to 2×10^8, 2×10^6, 4×10^5, 2×10^5 respectively, as shown in Figure 2.1.

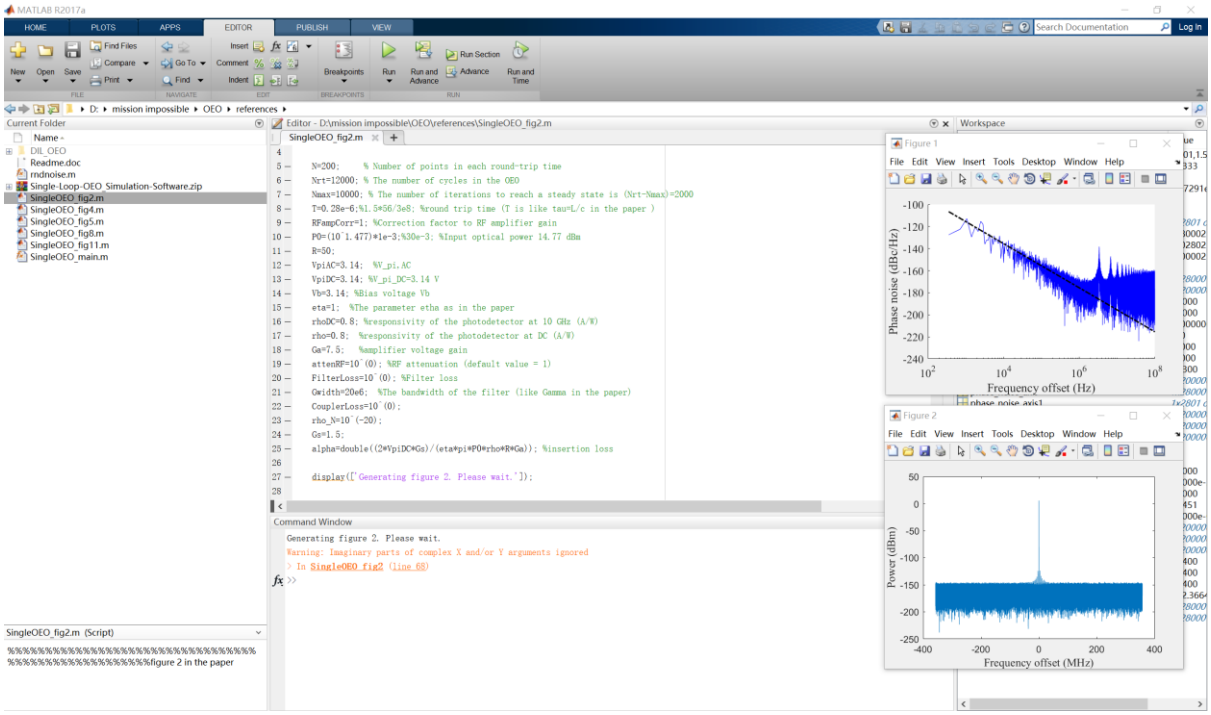

Figure 2.1 Single-loop OEO modelling simulation running by MATLAB.

When the different length of the single-loop OEO is set, the phase noises are calculated and are shown in Figure 2.2. It indicates that the phase noise decreased and the frequency space range reduced when the fiber line became longer. Besides, the phase noise level at each frequency is different in each simulation because the noise is random.

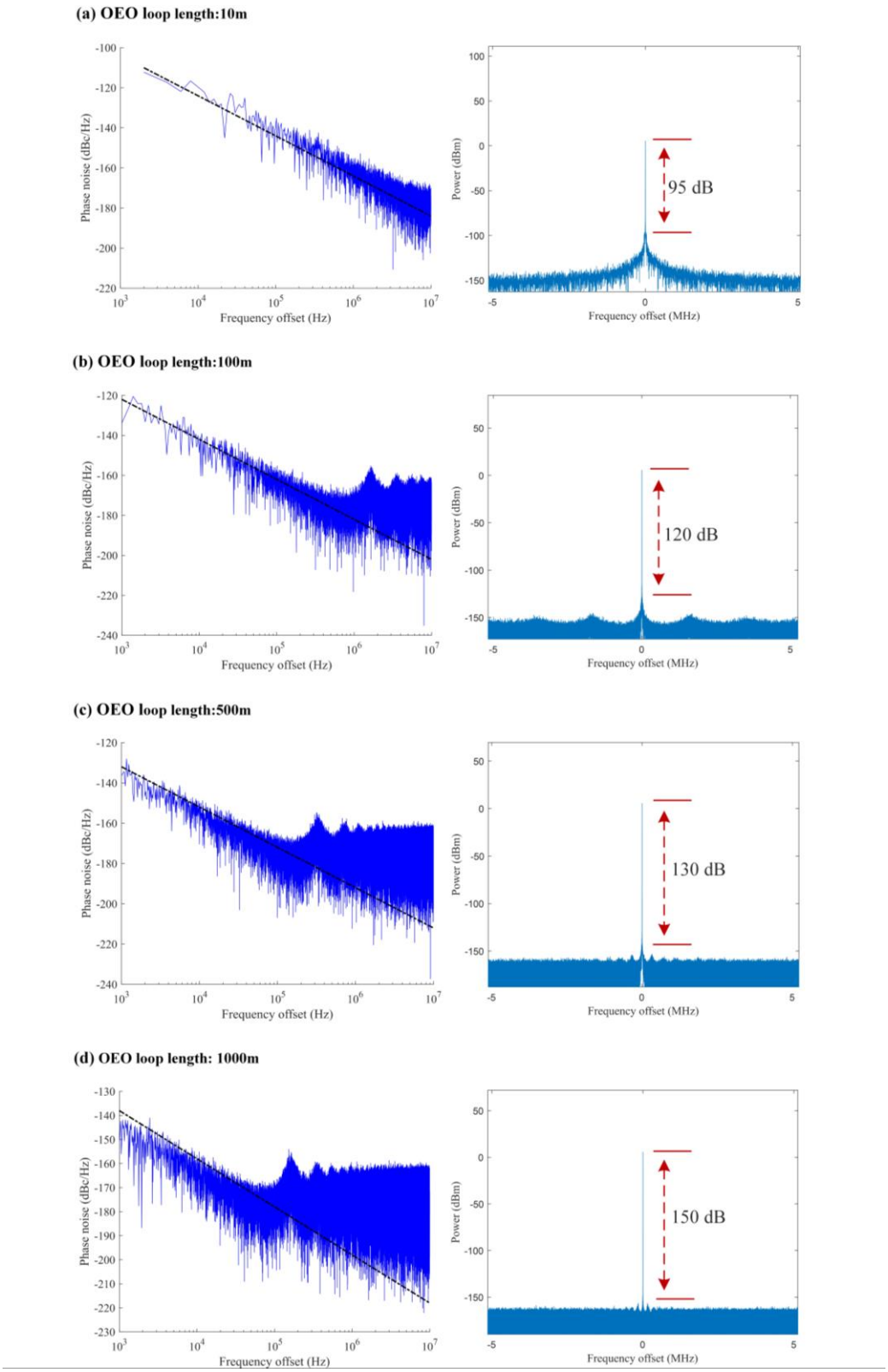

Figure 2.2 Phase noise of generated signal by single-loop OEO based on different length loop. (a) 10m fiber: phase noise -125 dBc/Hz @10kHz, suppression ratio is larger than 95 dB. (b) 100m fiber: phase noise -140 dBc/Hz, suppression ratio is larger than 120 dB. @10kHz (c) 500 fiber: phase noise -150 dBc/Hz @10kHz, suppression ratio is larger than 130 dB. (d) 1000 fiber: phase noise -160 dBc/Hz @10kHz, suppression ratio is larger than 150 dB.

2.3. Experiment Setup

The OEO is implemented using commercial optical and optoelectronic components.

EOM is a device used in optics and photonics to modulate the phase, amplitude, or polarization of light with an electrical signal. EOMs exploit the electro-optic effect in which the refractive index of a material changes in response to an applied electric field. EOMs can provide very fast modulation speeds, often in the gigahertz range, making them essential for many modern optical applications [83][86].

The PD is a device that converts light into an electrical signal. These devices operate based on the principle of photoelectric effect, wherein the absorption of photons leads to the excitation of electrons, subsequently producing an electrical current or voltage. Photodetectors play a crucial role in various applications such as telecommunications, imaging, medical diagnostics, and many scientific instruments [87][89].

The low noise amplifier (LNA) is an electronic amplifier used primarily to amplify signals without adding significant noise. The purpose of an LNA is to improve the (SNR of received signals, which is crucial in many communication and instrumentation systems. LNAs play a crucial role in many electronic systems, ensuring that weak signals can be detected and processed without being swamped by noise. LNAs are frequently used in the front end of radio receivers, satellite communication systems, radar systems, and other systems where weak signals need to be amplified without degrading their quality. The primary characteristics of an LNA include its gain (how much it amplifies the signal), noise figure (how much noise it adds to the signal), input and output impedance (for matching to source and load), and linearity [90].

The EBPF allows signals within a specific frequency range to pass through while attenuating (reducing) the signals outside of this range. It is defined by its passband

(the range of frequencies that are allowed to pass) and its stopband (the range of frequencies that are attenuated or rejected) [92].

In our experiments, the light is immitted from a mode-locked laser (MLL) chip, and then modulated by a $LiNbO_3$ MZM (FUJITSU FTM7960EX) with a 3dB optical bandwidth that exceeds 25 GHz. For detecting the optical signal in the linear response of PD, a tunable erbium doped fiber amplifier (EDFA) (AMONICS AEDFA-PA-35-B-FA) is implemented to provide an optical gain of 26 dB. Following by converting to RF microwaves through a PD (HP 11982A) that has 18GHz bandwidth from 3dB. To suppress unwanted modes, the EBFP is employed on the electrical loop, which has a bandwidth of 10 MHz at the central frequency of 10 GHz. After that, the electrical divider (or combiner) has a bandwidth from 7 GHz to 40 GHz, and a LNA (Connphy CLN-1G40G-4065-K) provides the gain of more than 35 dB for oscillating.

The spectrum and the phase noise of the microwave signal generated by the OEO are analysed by optical spectrum analyser (OSA) (Anritsu MS9710C) and electrical spectrum analyser (ESA) (Anritsu MS2840A), respectively. The open-loop frequency response of the OEO loop is measured using a network analyser (VNA) (Anritsu 4645B).

Chapter 3. Partially integrated coupled optoelectronic oscillator based on an Integrated Mode-Locked Laser

The optoelectronic oscillator (OEO) can generate high-performance radio frequency (RF) signals that are highly needed in optical communication and radar systems. An innovative work proposes a design method for a partially integrated coupled OEO. By employing a monolithic mode-locked laser (MLL) chip, the round-trip time of the OEO loop can be adjusted to tune the oscillating frequency. A high-quality (Q) storage element and the Verrier effect are implemented and integrated into the OEO system to improve the performance in terms of suppression and phase noise. In this case, the oscillating frequency of the microwave signal can be changed from 23.68 to 24.82 GHz, which phase noise at 10-kHz offset frequency is -100 dBc/Hz. Moreover, the side-mode suppression ratio reaches 40 dB. The robust design of this OEO system is advantageous for integration and thus exhibits potential for application in the miniaturization of microwave generation devices.

3.1. Design and fabrication of Mode-Locked Laser

A MLL is a type of laser that produces ultrashort pulses of light by actively controlling the phases of the laser modes. In a typical laser, modes of the laser cavity oscillate independently, producing a continuous wave (CW) output. In a mode-locked laser, the modes are synchronized in phase, resulting in extremely short pulses of light with durations on the order of picoseconds (10^{12} seconds) or femtoseconds (10^{15} seconds). The process of mode-locking involves synchronizing the phases of the longitudinal modes of the laser cavity. Basically, there are two main types of mode-locking: active and passive. In this experiment, a passively MLL system is designed and fabricated based on a linear cavity. To realize mode-locking within a laser cavity, the phases of

laser modes must be synchronized [93]. Seeing in Figure 3.1 (a), a 200 μm long forward distributed Bragg reflector (DBR-F) and a multimode interference reflector (MIR) constitute the linear laser cavity. In this laser cavity, a 500 μm long SOA provides the gain for laser emission by controlling injection currents. A 100 μm phase shifter (PS) is applied for wavelength fine-tuning. A shorter semiconductor optical amplifier (SOA) with reverse bias is configured as a saturable absorber (SA). A 50 μm rear DBR (DBR-R) is introduced to tune the pulse repetition frequency by altering the resonator round-trip time of the laser cavity. All these elements are monolithically integrated on an InP-based chip within a length of 1580 μm.

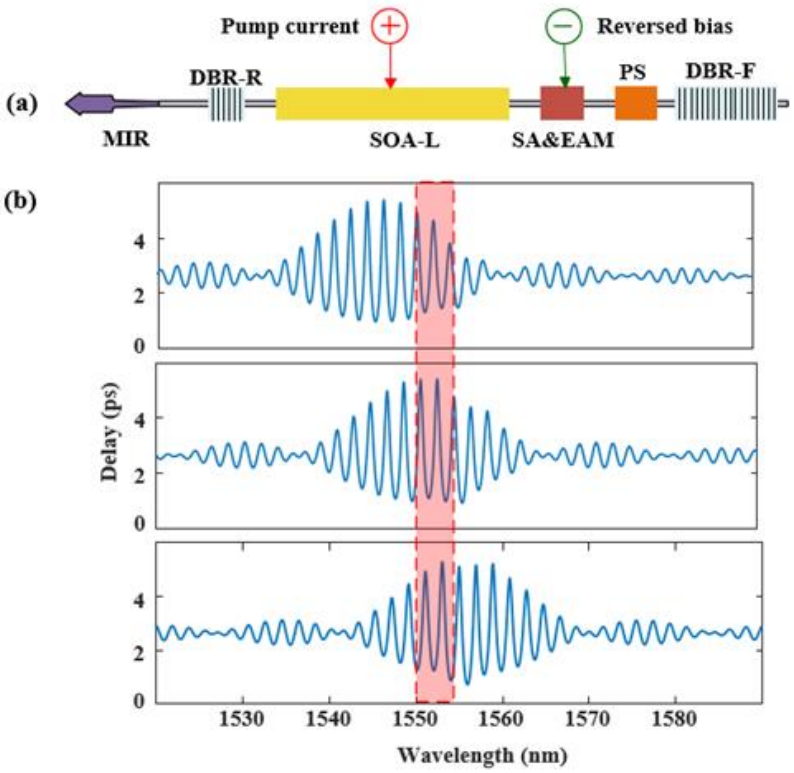

Figure 3.1(a) Block diagram of monolithic DBR laser. (b) Delay time distribution is adjusted by an effective refractive index of the DBR-R. (MIR: Multimode reflector. DBR-R: Distributed Bragg grating. SA: Saturable absorber. EAM: Electrical absorption modulator. DBR-F: Distributed Bragg reflector.)

With the setting of specific pump currents and reverse biases on the SOA and SA, the periodical transparency caused by saturation in the absorber and gain generates a pulse train. In the frequency domain, the MLL realizes an optical frequency comb

(OFC), whose frequency space is equal to the repetitive ratio of the pulse train. A microwave signal and a series of harmonics are obtained using photodetector (PD) to detect the optical envelope. Because of the limitation in PD bandwidth, it consistently obtains a microwave signal with a single fundamental frequency equal to the frequency space of the OFC, which is in turn. This design introduces a tunable dispersion by inserting a weakly DBR-R into the laser cavity, as shown in Figure 3.1 (a). The effective refractive index of the DBR-R is adjusted according to the currents injected. Consequently, the dispersion distribution of the DBR-R shifts. Because group delay in the other parts is kept constant, the total group delay in the laser cavity is adjusted by DBR-R. Figure 3.1 (b) illustrates variations in the group delay caused by the DBR-R. The group delay time distribution exhibits a redshift when the effective refractive index of DBR-R increases, as shown in the wavelength shift from the top to bottom panels of Figure 3.1 (b). In the refractive band for the laser cavity, the delay time distribution is adjusted by changing the current in DBR-R, as shown by the red strip in Figure 3.1 (b). As mentioned above, the frequency space of OFC is inversely proportional to the round-trip time of the laser cavity. Thus, the frequency of the generated microwave signal can be adjusted by changing the current in the DBR-R determined by the round-trip time in the laser cavity.

The passively MLL system has a significant drawback. In microwave generation, the jitter of the pulse train deteriorates the phase noise. In this study, it implemented optoelectronic feedback to overcome this issue. Firstly, an optoelectronic feedback loop is introduced to optimize the phase noise. The detected microwave signal is re-injected into the laser cavity after passing through an electrical amplifier. The microwave signal generated by optoelectronic feedback can also be tuned via dispersion in the laser cavity. In order to decrease the phase noise in the microwave

signal, a high-Q storage element could be introduced in the optoelectronic feedback loop, which typically comprises a single-mode fiber of a few kilometres' length. However, since the frequency space is inversely proportional to the length of single-mode fiber, there are tens of thousands of oscillating modes in the oscillating band simultaneously. To solve this problem and obtain a pure signal without mode hopping, the Vernier effect is employed to form a self-sustained filterless coupled optoelectronic oscillator (COEO) in a system. Subsequently, a spectrally pure RF signal was obtained.

Figure 3.2 illustrates the scheme of the setup for measuring the spectra of the MLL. Upon injection of the pump current into the gain medium (i.e., SOA) and setting of reverse biases in the SA, the MLL emits optical pulse trains. One part of this optical signal is sent to an optical spectrum analyser (OSA), whereas an electrical spectrum analyser (ESA) measures the other part after envelope detection.

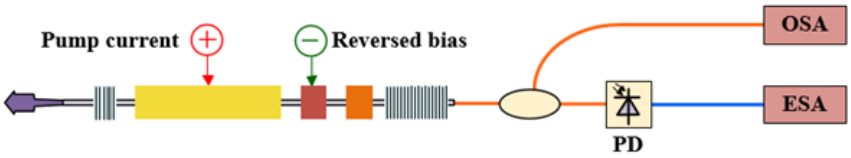

Figure 3.2 Scheme of the setup for measuring the spectra of the MLL. (PD: Photodetector. ESA: Electrical spectrum analyser. OSA: Optical spectrum analyser.)

In the experiment, the bias of SOA-S is reversed at –70 mV, and a short SOA can be configured as a SA. With 60 mA currents in SOA-L, DBR-F, DBR-R, and phase shifter (PS) are open-circuit. The OSA observes an optical comb with a frequency space of 24.8 GHz, and a microwave signal with a frequency of around 24.8 GHz is measured. The signal's optical and electrical spectra after out-chip photodetection are illustrated in Figure 3.3 (a) and (b), respectively. Upon intensifying the injected current in DBR-R from 0.07 mA to 2.5 mA, the round-trip time in the laser cavity is adjusted due to the shift in the dispersion curve of the DBR-R. Therefore, a microwave signal is generated

after photon detection, the frequency of which is continuously tuned from 23.75 GHz to 24.8 GHz, as shown in Figure 3.3(c).

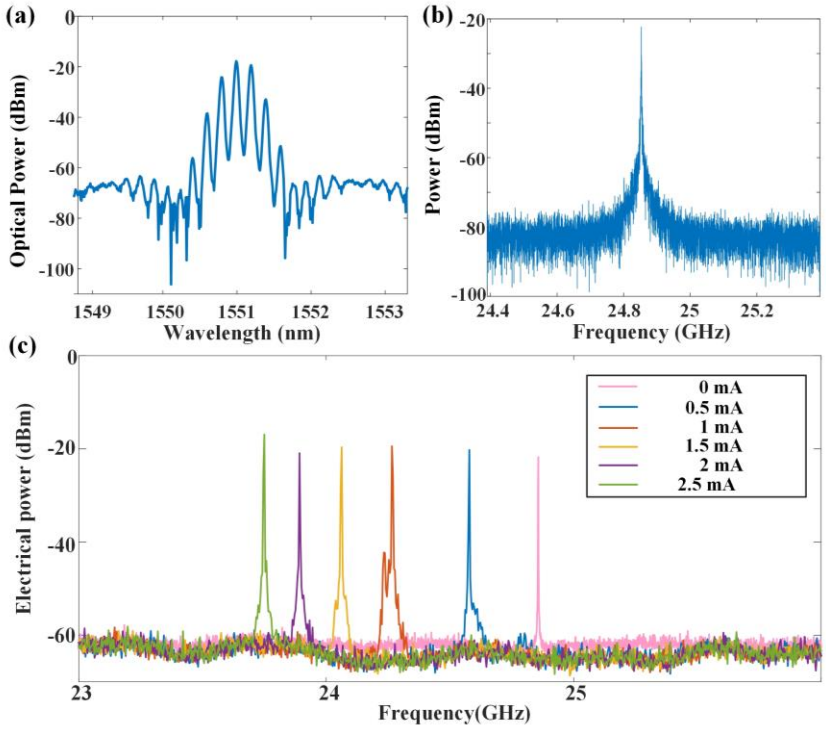

Figure 3.3 (a) Optical spectrum of DBR laser. (b) Electrical spectrum after out-chip photodetection. (c) DBR laser tuning from 23.75 GHz to 24.8 GHz.

3.2. Single-loop coupled optoelectronic oscillator

As mentioned before, the microwave signal directly generated by the MLL exhibits high phase noise, which is detrimental for a microwave source. Optical feedback or hybrid mode-locking needs to be introduced to improve the performance of the MLL. Optoelectronics provides a practical approach to realize that goal, as it can dramatically optimize the phase noise of generated microwave signals without additional microwave sources. Based on this technology, a scheme with an optoelectronic feedback loop is proposes, as shown in Figure 3.4. After the PD, a low noise amplifier (LNA) provides sufficient signal gain to stabilize the oscillation. The amplified signal with reverse bias is injected into the electrical absorption modulator

(EAM) through the microwave port (GPPO) on the package. The SA is reused as an EAM within the MLL.

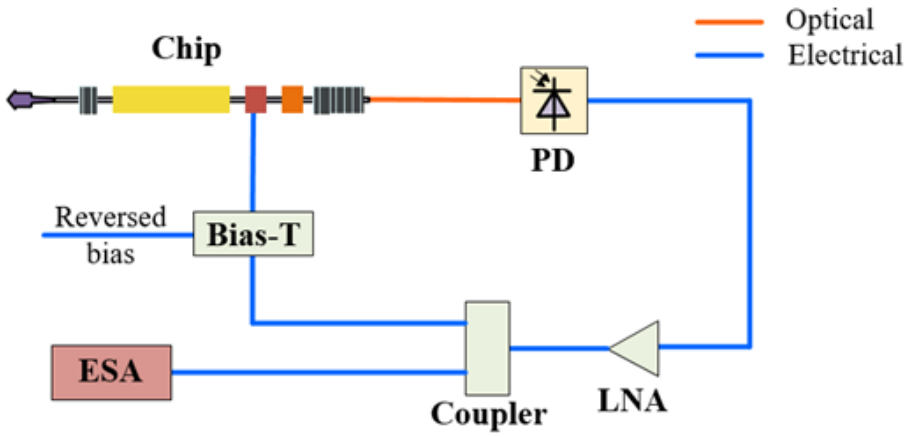

Figure 3.4 scheme of single loop optoelectronic feedback. (PD: photodetector. LNA: low-noise amplifier. ESA: Electrical spectrum analyzer.)

A pure microwave signal with 24.6 GHz frequency is generated when the optoelectronic feedback loop is closed, as shown in Figure 3.5 (a). As the optoelectronic feedback is another oscillating cavity with an optical length of approximately 47 meters, some side modes are detected in the ESA, whose interval frequency is 6.4 MHz. A stable microwave signal is achieved in this scheme, where the side-mode suppression ratio is larger than 40 dB, and its phase noise is approximately –80 dBc/Hz at an offset frequency of 10 kHz, as shown in Figure 3.5 (b). Similarly, the oscillating frequency is adjusted by altering the dispersion in the laser cavity. When the current in the DBR-R is changed from 0 mA to 2 mA, the oscillating frequency adjusts from 24.71 GHz to 23.91 GHz, as shown in Figure 3.5 (c). Meanwhile, the current injected into the PS is also altered to satisfy the phase condition of oscillation. The side-mode suppression ratio remains higher than 40dB for all oscillating frequencies, and the phase noise at 10kHz offset frequency is approximately -80 dBc/Hz. As discussed in section 1 and 2, a high-Q storage element is introduced into the optoelectrical feedback loop to improve the performance of the

generated microwave signal. However, the longer fiber may cause mode popping problems and difficulty realizing the ability of mode selection. Generally, there are two methods to solve this problem. Employing an electrical band-pass filter (EBPF) in the electrical part of OEO system is the first choice. However, this limits tunability because of its fixed central frequency and fabricating a high-Q filter at high frequency is difficult and expensive. Thus, this study proposes dual-loop optoelectrical feedback to solve this problem based on the Vernier effect. Because dual-loop OEOs substitute an EBPF to suppress unwanted spur modes, polarization controllers (PC) are configured for the maximum suppression, which is illustrated detailed in the next section.

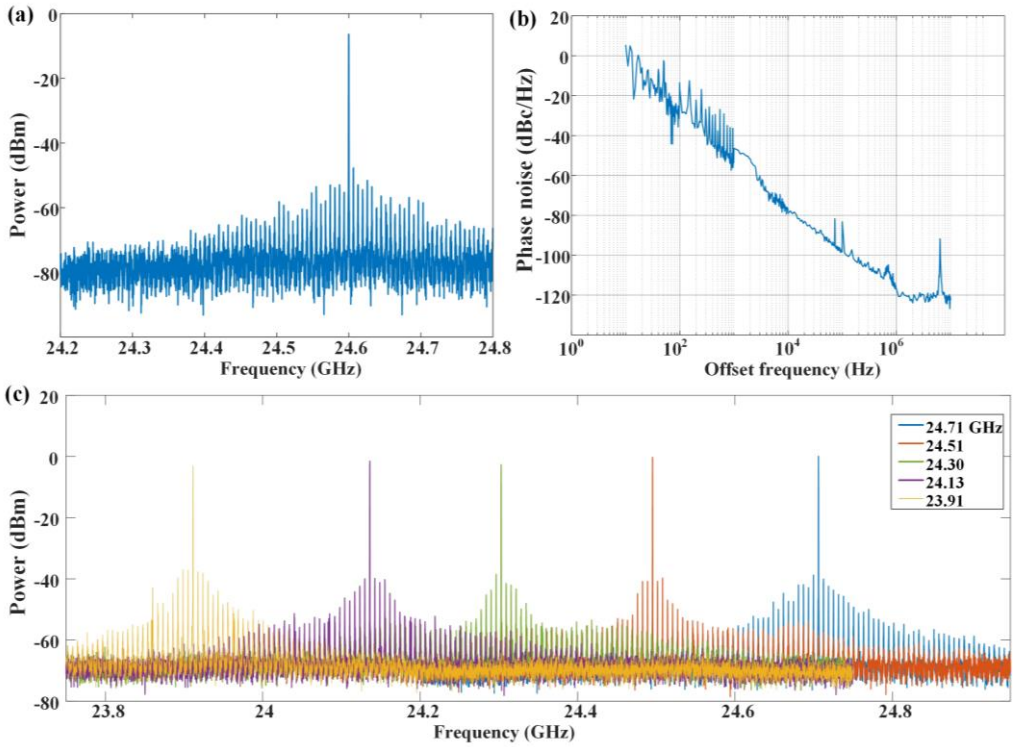

Figure 3.5 (a) Spectra of microwave signal generated by single-loop COEO. (b) Phase noise of the generated signal. (c) Oscillating frequency tuned from 24.71 GHz to 23.91 GHz.

3.3. Partially integrated dual-loop coupled optoelectronic oscillator

In our experiment, dual-loop OEOs with different loop lengths are implemented to configure self-sustained filterless COEOs. The longer loop determines the phase noise of OEOs, whereas the shorter loop determines the mode space, as shown in

Figure 3.6. In this experiment, two single-mode fiber (SMF) with lengths of 1.063 km and 5.046 km are implemented to introduce different loop-time delays. This configuration can both realize high-Q and mode selection.

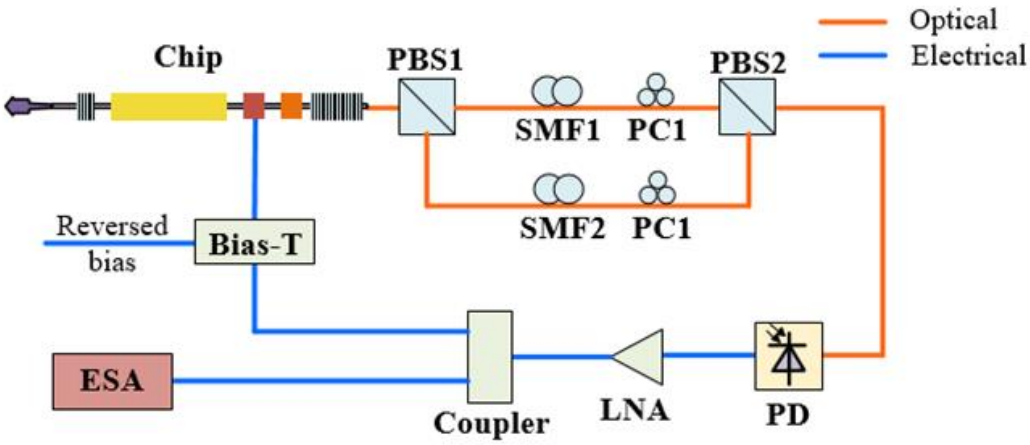

Figure 3.6 Configuration of Dual-loop OEO. (SMF: Single-mode fiber. PC: Polarization controller. PBS: Polarization beam splitter. LNA: Low-noise amplifier. ESA: Electrical spectrum analyzer.)

Such filterless OEO generates a RF signal with a frequency of 24.82 GHz, as shown in Figure 3.7(a) and (b). The suppression ratio is larger than 47 dB within a spectrum span of 1 MHz (resolution bandwidth: 10 kHz, video bandwidth 3 MHz, Anritsu MS2840A). The round-trip time in the laser cavity is altered by tuning the injected current in DBR-R. In the open-loop system, the pulse repetition frequency of the pulse wave laser is shifted, which results in a tunable stable oscillating frequency output from OEOs, as shown in Figure 3.7 (c). Simultaneously, DBR-F, Polarization beam splitter (PBS), and PC are controlled to enhance the oscillating signal quality at different frequencies. In the experiment, a series of microwave signals ranging from 23.68 GHz to 24.82 GHz are generated.

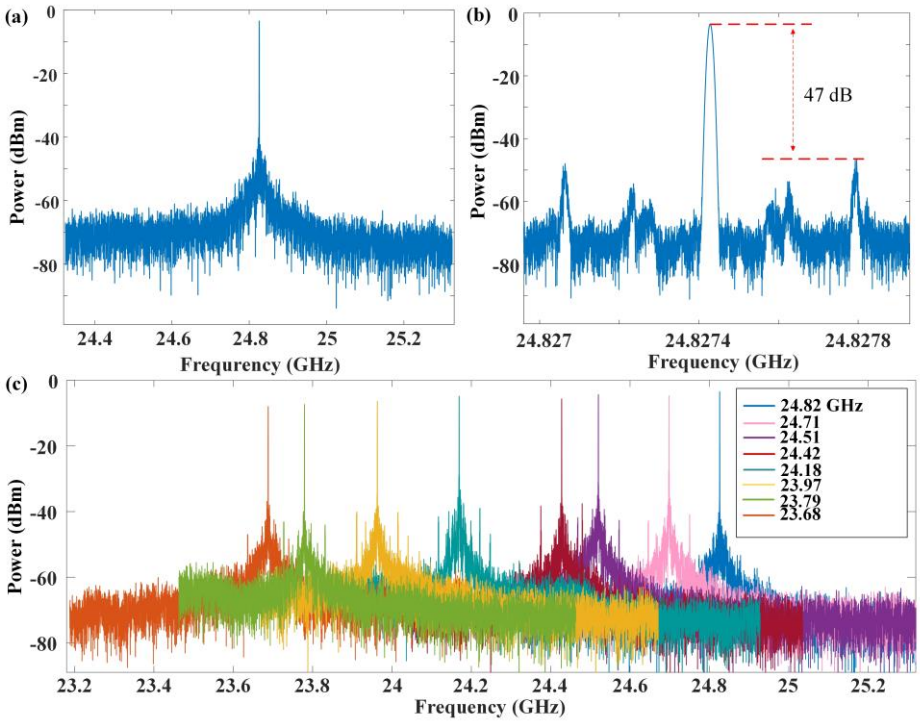

Figure 3.7 Electrical signal generated by OEO based on the dual-loop system. (b) Details of the generated signal. (c) Tunable range of generated signals by proposed OEO.

As can be seen, the tunable range of single-loop COEO is slightly different from dual-loop COEO, which is due to the principle that oscillating frequency is related to the loop length of OEO, the bias setting of the modulator and the central frequency of the filter.

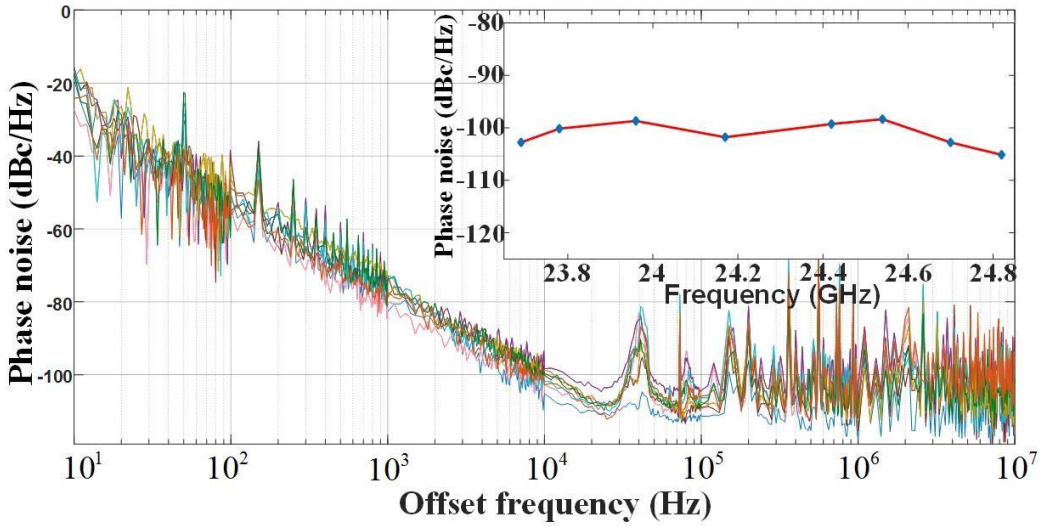

Figure 3.8 Phase noise for generated signals at different frequencies and phase noise of oscillating signals at 10 kHz offset frequency.

The phase noise values of each oscillating frequency signal are investigated. The phase noise of oscillating signals is around –100 dBc/Hz at the offset frequency of 10 kHz, as shown in Figure 3.8. The performances of generated signals based on chip-OEOs are stable across different oscillating frequencies. No oscillation mode hopping is detected during the observation (which exceeds 20 minutes). The oscillation performances can be optimized by introducing parity-time (PT) symmetry into the scheme, which will be demonstrated in the next studies.

3.4. Conclusion

This chapter introduces a microwave signal source by incorporating a COEO configuration to enhance the performance of the MLL. To streamline the RF source, a SA is introduced into the laser cavity, serving a dual purpose by configuring the proposed MLL and compacting the RF source. This SA, additionally repurposed as the EAM, obviates the need for an extra modulator, a characteristic feature of traditional COEOs. Based on the developed MLL chip, a single-loop OEO is firstly proposed and the narrow-band gain spectrum of the MLL is used to realize a stable oscillation with single-mode. A microwave signal is generated whose frequency tuning

range is 23.91-24.71 GHz and the best phase noise is -80 dBc/Hz (@10 kHz). Then, a dual-loop COEO scheme designed to enhance the oscillation performance, particularly with regard to phase noise. Experimental validation showcases the successful generation of microwave signals, characterized by a phase noise value of approximately -100 dBc/Hz at a 10 kHz offset frequency and an oscillation frequency tuning range spanning from 23.68 GHz to 24.82 GHz. This underscores the feasibility of implementing compact and cost-efficient OEOs as RF signal generators with tunable capabilities. Consequently, the proposed integrated COEO system, featuring the utilization of a MLL, presents an approach for the downsizing of RF signal sources while maintaining tunability, as show in Figure 3.9.

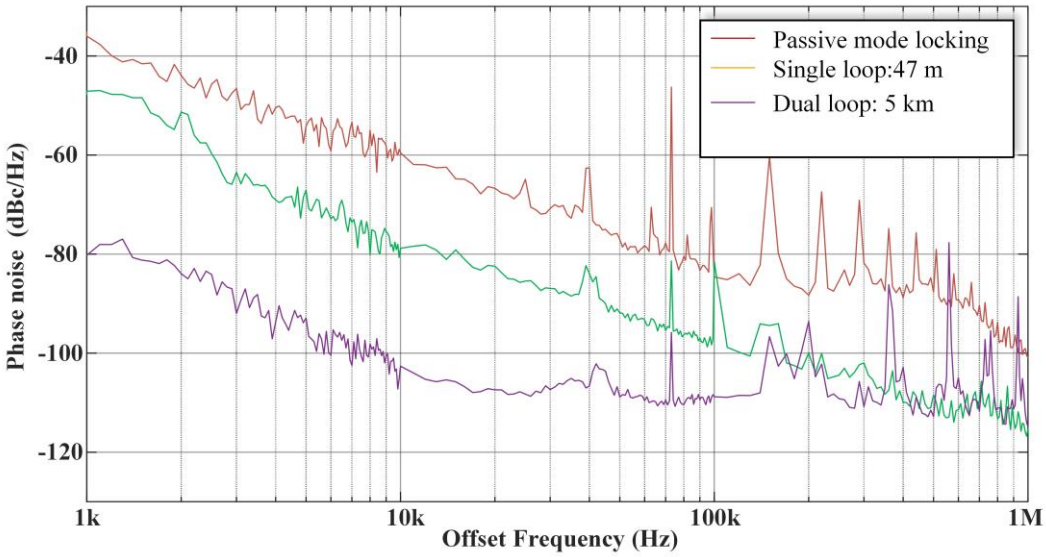

Figure 3.9 A comparative analysis of phase noise in microwave signals produced by OEO with diverse architectures.

Chapter 4. Parity-Time Symmetric Optoelectronic Oscillator

The advancement of the next-generation Opto-Electronic Oscillators (OEOs) poses considerable challenges in establishing stable and ultrahigh-quality (Q) mode selection mechanisms for extended optical feedback loops. Moreover, the implementation of Parity-Time Symmetry (PT-symmetry) in OEOs proves to be more intricate, given the stringent requirements on on-chip lasers and modulators in a hybrid integration configuration. Originating from non-Hermitian quantum mechanics, PT symmetry has been extensively investigated as a means to ensure stable single-mode oscillation in OEOs while circumventing the formidable challenges associated with ultrahigh-Q filters. Leveraging the capabilities of emerging Photonic Integrated Circuit (PIC) technology, this study introduces a tunable PT-symmetric OEO employing an integrated mode-locked laser, representing a notable advancement aimed at reducing the footprint of OEOs. The implemented system achieves the generation of a stable single-mode oscillating signal at 24.5 GHz, accompanied by a phase noise of -108 dBc/Hz at a 10 kHz frequency offset. Notably, a tunable frequency range spanning from 24 to 25 GHz is realized through the manipulation of injection currents into the intricately designed on-chip linear laser cavity. This work marks a pivotal breakthrough in the conceptualization of integrated microwave photonic devices, facilitating the practical application of the fundamental physical theory of PT symmetry within the information industry.

4.1. Scheme of Parity-Time Symmetry Optoelectronic Oscillator

Figure 4.1 illustrates the scheme of the PT-symmetric OEO based on the integrated mode-locked laser. The optical frequency comb (OFC) is transmitted through a fiber coil to form long-feedback loops. A polarization modulator (PC) and a polarization

beam splitter (PBS) are used to configure two identical and coupled loops in two orthogonal polarization states, acting as the gain and the loss loop for the PT-symmetry, respectively. Next, a tunable delay line introduces a π phase shift (i.e., half-wavelength delay) between two loops for the oscillating microwave signal. The outputs of the two loops are detected in a balanced photodetector (BPD) with a responsivity of 0.6 A/W, and the recovered microwave signal is sent back to the on-chip saturable absorber (SA) to close the OEO loops. It is highlighted that the SA in the PIC enables a hybrid mode-locking, thanks to its twofold function for saturated absorption and electro-absorption modulation. Besides, the oscillating frequency of microwave beating notes can be tuned, while adjusting the currents applied to the distributed Bragg reflector (DBR-R).

Figure 4.1 (a) The microscope photo of the six-section PIC. The six-section PIC is the main body, including a multi-mode interference reflector (MIR), a rear front distributed Bragg grating (DBR-R), a long semiconductor optical amplifier providing gain (SOA-G), a saturable absorber or electro-absorption modulator (SA/EAM), a phase shift (PS), and a front distributed Bragg grating (DBR-F). (b) Schematic diagram of integrated PT-symmetric OEO. (SMF: Single-mode fiber. PC: Polarization controller. PBS: Polarization beam splitter. TDL: Time delay line. BPD: Balanced photodetector. LNA: Low-noise amplifier. ESA: Electrical spectrum analyzer.)

4.2. Experiment Result

Typically, an ultrahigh-Q electrical or photonic filter is inserted into the oscillation loops to select a single, stable oscillating mode among thousands of candidate modes.

Nevertheless, the bandwidth of such an ultra-narrow filter should be less than the mode spacing which is hardly to achieve in the microwave band (e.g., beyond 20 GHz). Therefore, the PT symmetry can be explored here in the integrated OEO. By adjusting the polarization controller (PC), the gain and the loss are manipulated in the same magnitude for the two feedback loops with orthogonal polarization states to fulfill the requirement of the PT-symmetry. Then, breaking the PT-symmetry leads to the generation of a single-tone microwave signal at 24.5 GHz, defined by the mode spacing of the passive mode-locking. As shown in Figure 4.2, the spectra of the generated microwave signal are recorded in different spans, and the side mode suppression ratio is estimated to be higher than 20 dB. The oscillating frequency is slightly different from the central frequency of free-running mode-locked lase (MLL), since the feedback voltages on the SA results in the changes of round-trip time and the selected oscillating mode locks MLL. More importantly, to clearly demonstrate the stability enhancement of the single-mode oscillation, the generated microwave signal is monitored continuously exceeding 10 minutes by using a spectrum analyser. In addition, the Vernier effect and the fast power limiting also can be configured as two mode-selection methods for implementing tunable OEOs based on mode-locked laser [19][80].

Figure 4.2 Electrical spectra of microwave signal generated by the PT-symmetric OEO. (Measured spectra of the microwave signal at 24.5 GHz generated by the integrated PT-symmetric OEO.) The spectra are measured with a span of (a) 100 MHz with RBW of 100 kHz. (b) 10 MHz with RBW of 10 kHz. (c) 1 MHz with RBW of 1 kHz. (d) 100 kHz with RBW of 1 kHz.

The phase noise of the generated single-tone microwave signal is measured to be -108 dBc/Hz at the 10-kHz offset frequency, as shown in Figure 4.3. For the simplicity of comparison, other phase noises are measured for different fiber loop lengths of 46.68 m, 1.1 km, and 5.09 km, which are -76.96, -102.4, or -108 dBc/Hz. These results follow the trend that the phase noise drops with the increase of the loop length. An enhanced phase noise is achieved by using a long loop, in contrast to the phase noise of a 24.5-GHz microwave signal generated by a commercial microwave source (Anritsu MG3694C). Moreover, the single-mode oscillating signal generated from the PT-symmetric OEO outperforms the microwave signal directly generated from the passive mode-locked laser, by a phase noise enhancement of 50 dB. Due to the absence of an external reference clock, the stability of the generated OFC is slightly affected and thus the performance of phase noise is limited in the PT-symmetric OEO. Although a longer feedback loop would optimize the phase noise further, the frequency space range (FSR) remarkably drops, leading to instability for breaking PT symmetry

and a high-resolution gain and loss controller for single-mode selection. In order to reduce the phase noise further, jitter reduction for passively mode-locked laser through optical feedback will be a potential solution [81].

Figure 4.3 Measured phase noises of the generated microwave signals. The PT-symmetric OEO was formed by using three different loop lengths of 46.68 m,1.1 km, and 5.09 km. The corresponding phase noises are −76.96, −102.4, and −108 dBc/Hz at an offset frequency of 10 kHz, respectively. For the purpose of comparison, the phase noises of a microwave signal generated by a commercial microwave source and of the microwave beating note directly generated from the passive mode-locked laser are also presented, indicating a phase noise improvement of 7.37 dB or 50 dB for the PT-symmetric OEO, respectively.

Tunable characteristics can be achieved in the PT-symmetric OEO by adjusting the round-trip time of the integrated mode-locked laser. In the PIC, the round-trip time of the passive mode-locked state can be slightly tuned by adjusting the currents into the DBR-R. When the PT-symmetry is broken for different central frequencies of gain, stable single-mode oscillations at different microwave frequencies are achieved. A tunable single-mode microwave signal is thus generated from the PT-symmetric OEO based on the mode-locked laser, as shown in Figure 4.4. Its tunable frequency ranges from about 24 to 25 GHz. The phase noises are lower than −108 dBc/Hz at the 10-kHz offset frequency and the fluctuation of phase noise is about 2 dB within the whole tunable frequency range.

Figure 4.4 Tunable microwave signal generated by the integrated PT-symmetric OEO. (a) Spectra of microwave signals at 24.02 GHz, 24.50 GHz, 24.96 GHz and (b) Phase noises of three microwave signals respectively.

4.3. Conclusion

A tunable PT-symmetric OEO based on an integrated MLL is proposed and demonstrated for the first time. The PIC enables on-chip continuous-wave laser generation, mode-locking, electro-optic modulation, and frequency tuning, for the PT-symmetric OEO. The PT symmetry is achieved by configuring two identical feedback loops with orthogonal polarization states, one having a gain and the other having a loss in same magnitude. By breaking the PT symmetry, a stable single-tone microwave signal at 24.5 GHz was experimentally demonstrated and its phase noise was estimated as −108 dBc/Hz at a 10 kHz frequency offset. Compared to conventional OEOs with a long fiber loop, the partially integrated PT-symmetric OEO reveals greatly enhanced stability for the single-mode oscillation in the absence of an ultrahigh-Q filter. In addition, the PIC provides a tunable frequency range from about 24 to 25 GHz for single-tone oscillation, while keeping the phase noise around −108 dBc/Hz. This work emerges as a new paradigm to develop next-generation integrated OEOs using filter-less mode selection in the microwave photonic field, and to transfer the fundamental physical theory (i.e., PT symmetry) into practical applications, powered by modern advanced technologies (i.e., PIC and microwave photonics).

Chapter 5. Future work

5.1. New requirement of the local oscillator in 5G and beyond wireless network

In the concluding section, the performance metrics of the Opto-Electronic Oscillator (OEO) are presented. It is imperative to delineate the specific criteria for the Local Oscillator (LO) when contemplating the utilization of OEOs in the 5G wireless network and subsequent generations. In accordance with the standards promulgated by the 3rd Generation Partnership Project (3GPP), this necessitates an exploration of the novel requirements that have emerged in the landscape of 5G wireless networks.

Contemporary imperatives within wireless networks underscore the critical significance of frequency accuracy and Error Vector Magnitude (EVM) in receivers. These parameters directly correlate with the frequency stability and phase noise characteristics of the LO. The ensuing sections are dedicated to a thorough examination aimed at elucidating the specific requirements of the LO, tailored to align seamlessly with the distinctive attributes inherent in 5G wireless communication systems.

Moreover, guided by the established benchmarks of 5G standards, the subsequent discourse delves into the formulation of Key Performance Indicators (KPIs) for the LO within the prospective domain of 6G wireless networks. This forward-looking analysis serves as a foundational framework for future investigations (Chapter 5).

5.1.1. Characteristics of wireless network

5.1.1.1. 5G New Radio in Frequency Range 1

ETSI TS 138 104 provides the requirements for the frequency synchronization applied to 5G networks [78]. The standard states that a wide area BS should use a single-

frequency source with an absolute accuracy better than 0.05 ppm for both microwave generation and clocking the time base, while the same source should be used for all carriers of the base station (BS), and the absolute accuracy requirement is relaxed to 0.1 ppm for the medium range and local area BS class. The synchronization requirement of 0.05 ppm has become not only a milestone of mobile-technology-driven requirements for synchronization but also the primary driving force behind recent synchronization studies.

Table 3 Frequency error minimum requirement for 5G NR in FR1 (410 MHz – 7125 MHz)

BS class	Accuracy
Wide Area BS	±0.05ppm
Medium Range BS	±0.1ppm
Local Area BS	±0.1ppm

Table 4 EVM requirement for 5G NR Sub-6G in FR1 (410 MHz – 7125 MHz)

Modulation scheme	Required EVM
QPSK	17.5%
16QAM	12.5%
64QAM	8%
256QAM	3.5%

ETSI TS 138 104 also provides the requirements for the error vector magnitude (EVM) levels of each new radio (NR) carrier for different modulation schemes applied to 5G networks in Frequency Range 1 (FR1) [78][79]. The standard states that the EVM should be better than 17.5% for quadrature phase shift keying (QPSK) and 3.5% for 256 quadrature amplitude modulators (QAM), as listed in Table 4.

5.1.1.2. 5G New Radio in Frequency Range 2

ETSI TS 138 104 also defines the requirements of frequency synchronization in the mm-wave band. Though the requirement of frequency error in the millimeter-wave range is also 0.05ppm for wide-area BS, it is harder for a mm-wave oscillator to achieve the performance.

Table 5 Frequency error minimum requirement for 5G NR in FR2 (24250 MHz–52600 MHz)

BS class	Accuracy
Wide Area BS	±0.05ppm
Medium Range BS	±0.1ppm
Local Area BS	±0.1ppm

ETSI TS 138 104 also defines the requirements for the EVM levels of each NR carrier for different modulation schemes in the mm-wave band. The standard states that the EVM should be better than 17.5% for QPSK and 8% for 64 QAM, as listed in Table 6.

Table 6 EVM requirement for 5G NR in FR2 (24250 MHz–52600 MHz)

Modulation scheme	Required EVM
QPSK	17.5%
16QAM	12.5%
64QAM	8%

5.1.2. Requirement of frequency stability

5.1.2.1. Requirement of frequency stability

The modulated signal is up-converted (or down-converted) from the baseband to the RF band (or from RF to the baseband) in BS by mixing with the LO. The frequency stability of LO is the main factor that directly affects the frequency accuracy of the wireless network. The frequency shift of each NR carrier caused by the LO should be

lower than the accuracy given in Tables 3 and 5 observed over 1ms. And the frequency shift f_s in ppm is calculated by dividing carrier frequency f_C into f_s,

$$f_s(ppm) = \frac{10^6 * f_s(Hz)}{f_c} \quad \text{(eq.11)}$$

Based on this equation, it can analyze the criterion of frequency accuracy for a specific carrier. For example, if the carrier frequency is 26 GHz, the frequency shift of the LO should be lower than 1.3 kHz observed over 1 ms.

5.1.2.2. Requirement of phase noise

The 31 dB signal-to-noise ratio (SNR), the analog-to-Digital converter (ADC) quantization noise, the ADC clock jitter, and the phase noise of LO are the important effects resulting in the EVM of the wireless network [98]. To evaluate the EVM caused by the phase noise, it needs to analyze how the phase jitter results in the EVM. In the receiver, the QAM or QPSK signal is represented as an in-phase and quadrature message with respect to the carrier, which can be written as:

$$x(t) = m_I(t)\cos(\omega_{RF}t) + m_Q(t)\sin(\omega_{RF}t) \quad \text{(eq.12)}$$

Where $m_I(t)$ and $m_Q(t)$ represent the in-phase and quadrature amplitude, ω_{RF} is the carrier frequency. In polar coordinates, the received signal can be written as:

$$x(t) = A(t)\cos(\omega_{RF}t + \phi(t)) \quad \text{(eq.13)}$$

where $A(t) = \sqrt{m_I^2(t) + m_Q^2(t)}$ and $\phi(t) = \tan^{-1}(m_I(t)/m_Q(t))$ are the amplitude and the phase.

The received signal is mixed with the LO where a phase jitter θ is added to $\phi(t)$. The mixed signal in in-phase and quadrature vector can be written as:

$$\begin{aligned}\overrightarrow{m_I}(t) &= 2A(t)\cos(\omega_{RF}t+\phi(t))\cos(\omega_{LO}t+\theta) \\ &= A(t)\cos(\phi(t)-\theta)\end{aligned} \quad \text{(eq.14)}$$

$$\begin{aligned}\overrightarrow{m_Q}(t) &= 2A(t)\cos(\omega_{RF}t+\phi(t))\sin(\omega_{LO}t+\theta) \\ &= A(t)\sin(\phi(t)-\theta)\end{aligned} \quad \text{(eq.15)}$$

Where ω_{LO} is the frequency of the LO. Assuming that the receiver is homodyne, $\omega_{LO}=\omega_{RF}$. The constellation for received IF signal is expressed as:

$$\begin{aligned}S_{real} &= \overrightarrow{m_I}(t)+\overrightarrow{m_Q}(t) \\ &= A(t)[\cos(\phi(t)-\theta)+j\sin(\phi(t)-\theta)] \\ &= A(t)e^{j(\phi(t)-\theta)}\end{aligned} \quad \text{(eq.16)}$$

The real constellation minus the ideal constellation is the error of constellation, which can be written as:

$$\begin{aligned}S_{error} &= S_{real}-S_{idal} \\ &= A(t)e^{j\phi(t)}(e^{-j\theta}-1) \\ &= (\vec{m}_I+j\vec{m}_Q)(\cos\theta-1-j\sin\theta)\end{aligned} \quad \text{(eq.17)}$$

Where ideal constellation can be derived as $S_{idal}=A(t)[\cos\phi(t)+j\sin\phi(t)]=A(t)e^{j\phi(t)}$.

Furthermore, the error power caused by phase noise is expressed as:

$$\begin{aligned}P_{error} &= |S_{error}|^2 \\ &= (\vec{m}_I(\cos\theta-1)+\vec{m}_Q\sin\theta)^2 \\ &\quad +(\vec{m}_Q(\cos\theta-1)-\vec{m}_I\sin\theta)^2 \\ &= 2A^2(t)(1-\cos\theta)\approx\theta^2A^2(t)\end{aligned} \quad \text{(eq.18)}$$

Therefore, the EVM caused by the phase noise is approximated to the phase jitter,

$$\begin{aligned}EVM &= 100\%\times\sqrt{\frac{|S_{error}|^2}{|S_{ref}|^2}}=100\%\times\sqrt{\frac{A^2(t)\theta^2}{A^2(t)}} \\ &= 100\%\times\theta(rad)\end{aligned} \quad \text{(eq.19)}$$

The phase jitter θ of the LO is equal to the integration of phase noise power over the frequency range of interest, e.g., the area of the curve, A, as shown in Figure 5.2.

The lower bound of integration is set by the communication waveform time frame (generally 10-50 kHz), while the upper bound is set by the channel bandwidth (100 or 800 MHz).

It is customary to characterize an oscillator in terms of its single-sideband phase noise as shown in Figure 5.1. The actual curve of phase noise is approximated by several regions while each region has a slop of $1/f^x$. When x=0, it corresponds to the “white” phase noise region (slope=0 dB/decade), and x=1 corresponds to the "flicker" phase noise region (slope=–20 dB/decade). x=2, 3… are the offset frequencies close to the carrier frequency.

The individual power ratios are then summed and converted back into dB,

$$A = 10\log_{10}(A_0 + A_1 + A_2 + A_3) \qquad \text{(eq.20)}$$

Then the root-sum-square (RMS) phase jitter θ in radians is given by the equation:

$$\theta(rad) = \sqrt{2 \times 10^{A/10}} \qquad \text{(eq.21)}$$

Combing equations (eq.19) and (eq.21), the requirement of EVM in wireless networks is described by the requirement of the phase noise of the LO.

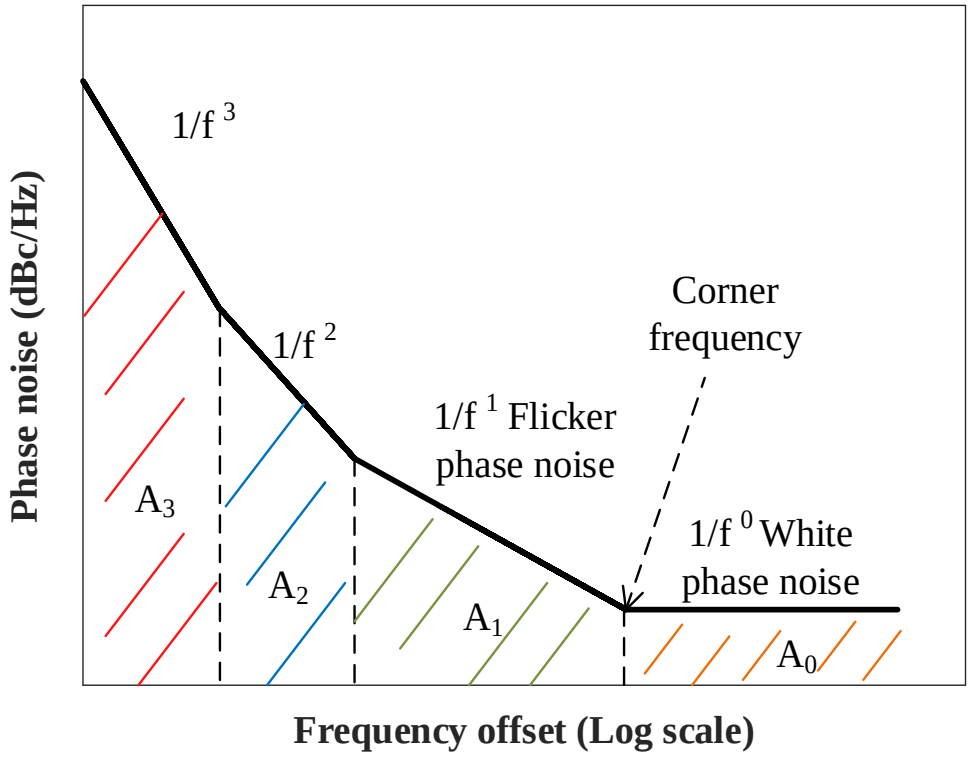

Figure 5.1 The customary characters of phase noise.

5.2. Terahertz Oscillator

5.2.1. Performance of Terahertz Oscillator

In the wake of the commercial deployment of 5G, research initiatives on the 6G wireless communication system have been initiated. Anticipating the need for higher frequencies to accommodate exceptionally high-speed data transmission in 6G, Terahertz (THz) technology emerges as a promising solution to address bandwidth limitations. Over the past years, several research endeavors have explored fully integrated THz systems, particularly in low-cost and reliable silicon technologies. This section provides a comprehensive review of noteworthy proposals in this domain, presenting their respective performance metrics in Table 7. In a seminal work by H. Jalili et al. [94], a wideband harmonic Voltage-Controlled Oscillator (VCO) with significant output power was introduced, leveraging a coupled standing wave oscillator. Executed in a 65-nm Complementary Metal-Oxide-Semiconductor (CMOS) process, the prototype chip covers a frequency band of 219-238 GHz, achieving an output

power of 3.4 dBm. The minimum measured phase noise is reported as -105.8 dBc/Hz at a 10-MHz offset frequency. Another noteworthy contribution by H. Wang et al. [95] outlines an approach to design compact and highly efficient THz fundamental oscillators, operational above half of the maximum frequency of the active device. Fabricated using 65-nm CMOS technology, a 213-GHz signal-ended and differential fundamental oscillator exhibited a phase noise of -93.4 dBc/Hz at a 1-MHz offset. Furthermore, a novel design of a harmonic VCO, implemented through the 130-nm SiGe processing, was proposed in [96]. This harmonic VCO generates THz signals with a tunable frequency ranging from 270.3 GHz to 279.3 GHz. The corresponding phase noise is measured as -81.2 dBc/Hz at a 1-MHz offset frequency for the central frequency of 275 GHz.

Table 7 Reviews of THz signal generation

Freq. (GHz)	P.N. @1MHz (dBc/Hz)	Area (mm2)	Tech.	Pow. (mW)	Ref.
229	-85.8	0.21	65-nm COMS	195	[94]
213	-93.4	0.0675	65-nm COMS	11.5	[95]
275	-81.2	0.022	130-nm SiGe	42.3	[96]

Freq. frequency, P.N. phase noise, Tech. technology, Ref. reference, Pow. power.

5.2.2. 6G key performance indicators

In consonance with the evolutionary trajectory observed in previous generations of wireless communication systems, the requisites for frequency synchronization and EVM in the forthcoming 6G era are anticipated to be elevated. While the precise technical specifications of 6G remain undetermined, the prevailing consensus underscores the utilization of millimeter-wave (mm-wave) and Terahertz (THz) frequency bands as pivotal for achieving enhanced data rates. This necessitates stringent criteria for frequency accuracy, with the requirement stipulating that the

frequency error of the mm-wave and THz carriers should be equal to or surpass 0.05 parts per million (ppm). In pursuit of achieving transmission rates in the terabits per second (Tb/s) range, it is posited that more advanced and efficient modulation formats will be employed within the mm-wave or THz frequency bands. Considering a hypothetical scenario where the mm-wave band adopts 256 QAM and the THz band utilizes 64 QAM, the stringency of the LO phase noise requirements for both mm-wave and THz bands becomes apparent. Consequently, a comprehensive set of Key Performance Indicators (KPIs) for the 6G wireless communication system is proposed, as delineated in Table 8.

Table 8 Performance requirements 6G era

Frequency band	Accuracy	EVM
mm-wave band	±0.05ppm	3.5%
THz band	±0.05ppm	8%

5.3. Local Oscillator distributed network: Optoelectronic Oscillator based Local Oscillators for 5G and Beyond

The development of the 5G communication system encompasses various new scenarios, incorporating both the evolution of contemporary 4G networks and the globally standardized radio access technology denoted as NR. As elucidated in preceding sections, the anticipated characteristics of 5G and subsequent networks involve higher carrier frequencies, broader bandwidths, and the adoption of more efficient modulation formats for access networks. Additionally, the pivotal role of network densification, marked by crowded cells, is widely acknowledged in the context of 5G and beyond networks. Consequently, the distribution and synchronization of LOs between a Baseband Unit (BBU) pool and an array of Remote Radio Units (RRUs)

emerge as critical technologies within the fronthaul network. The fiber-compatible architecture of OEOs presents itself as a potential solution to address the challenges associated with LO distribution and synchronization in the fronthaul network for 5G and beyond network.

5.3.1. Cooperative Radio Access Network architecture for 5G network

In response to the evolving demands for broadband and low-latency communication, the 5G technology introduces mm-wave frequencies to facilitate signal transmission at higher data rates. This necessitates a reduction in cell size to a scale of a few tens of meters due to the elevated carrier frequency and data rate. Consequently, the deployment of a denser network infrastructure becomes imperative, with numerous BS and access nodes (ANs) situated within confined spaces, including those mounted on outdoor roadside lamps, as depicted in Figure 5.1. Within the access network framework of 5G communication, the Cooperative Radio Access Network (C-RAN) architecture emerges as a fundamental technology. In the C-RAN configuration, the BS is partitioned into a BBU pool and RRUs, as illustrated in Figure 5.1. This segregated architecture affords enhanced resource utilization, improved energy efficiency, and reduced deployment costs by sharing baseband resources across multiple radio cells. The interconnection between the BBU pool and RRUs is established through a low-latency, high-bandwidth optical network. In the RRUs, the baseband signal undergoes amplification, up-conversion to the RF band through mixing with a LO, and subsequent emission through antennas. A prominent challenge in the C-RAN paradigm pertains to the stringent performance requirements of the LO, encompassing not only phase noise and frequency accuracy but also necessitating ultra-low-loss distribution and synchronization. The utilization of an Injection-Locked OEO presents itself as an effective methodology to meet these exacting requirements.

Leveraging the inherent characteristics of optical networks facilitates seamless distribution and synchronization between the BBU pool and RRUs. The schematic representation of the injection-locked Opto-Electronic Oscillator (IL-OEO) architecture between the BBU pool and RRUs is delineated in Figure 5.1, with the ensuing sections detailing the specific requirements and viable implementations of the constituent subsystems.

Figure 5.2: The scheme of the injection-locked OEO in wireless networks.

5.3.2. Description of injection locked Opto-Electronic Oscillator

Figure 5.2 provides a schematic depiction of an IL-OEO system. This configuration comprises a high-performance master OEO situated in the BBU pool, alongside a series of energy-efficient OEOs deployed within RRUs. Interconnected by low-latency and low-loss optical fronthaul networks, the master OEO generates mm-wave signals distributed to slave OEOs in RRUs. The synchronization of phases between the

master and slave loops is achieved by injecting a portion of the master-loop signal into the slave loop, resulting in synchronized slave OEOs with low phase noise.

As expounded in Chapter 2, theoretical frameworks and experimental demonstrations of IL-OEO have been developed in previous research endeavors [32][82]. IL-OEO showcases ultra-low phase noise characteristics in both low-Q oscillators and high-Q oscillators. Previous studies have observed that the phase of the slave loop locks to the phase of the master loop when the offset frequency is below the Leeson frequency. Beyond this frequency, the slave loop signal plateaus, while the master loop's signal progressively diminishes with increasing offset frequency. Notably, the Leeson frequency experiences blue shifts in correlation with the master-to-slave injection ratio, thereby reducing the phase noise of the slave loop at high offset frequencies.

To align with the specifications of LOs in the 5G and beyond network, several considerations specific to IL-OEO are imperative. The master OEO is expected to exhibit ultra-low phase noise and high-frequency accuracy, whereas the slave OEO must prioritize energy efficiency, module size, and deployment cost.

In Chapter 2, it is discussed that the phase noise of the IL-OEO is inversely proportional to the fiber length. Therefore, an extended fiber length is imperative for the master OEO. Various IL-OEOs with low phase noise are reviewed in Table 1. Additionally, frequency accuracy or stability is identified as a critical performance metric for the master OEO. Due to the sensitivity of the optical fiber to stress and temperature, oscillating frequency shifts can compromise long-term frequency stability. To address this concern, proposed methods such as temperature-insensitive fibers, thermal stabilization, and phase-locked loops (PLLs) have been demonstrated. Notably, D. Eliyahu et al. proposed a high-Q and stable OEO system wherein resistive heaters and temperature controllers thermally stabilize the optical fiber and the narrow

band-pass microwave filter [97]. This stabilization improves the frequency stability of the free-running OEO to 0.02 ppm, and the frequency versus temperature slope significantly enhances compared to non-thermally stabilized systems. By locking the OEO to a standard reference, a 10 GHz signal is generated with a phase noise of -143 dBc/Hz at the 10 kHz offset frequency. In a separate approach [98], Y. Zhang et al. demonstrated that a single-loop OEO achieves long-term frequency stability through PLL technology. This implementation yields a highly stable 3-GHz microwave signal with a phase noise of -65 dBc/Hz at a 10-Hz offset frequency and a low-frequency stability for an average time of 1000 s. Conversely, the slave OEO demands efficient power consumption, compact size, and economical cost. Traditional OEOs are hindered by bulky dimensions and high-power consumption, presenting challenges in meeting the requirements of the 5G and beyond network. Fortunately, with the advancements in PIC technology, integrated OEOs on various PIC platforms have emerged, offering a compact and easily manageable implementation. LOs based on integrated OEOs exhibit the potential to significantly reduce footprint and cost while substantially enhancing stability and energy efficiency, thereby constituting a valuable contribution to the future wireless network landscape.

Reference

[1] Seeds A J and Williams K J, “Microwave photonics,” *J. Light. Technol.*, vol. 24, no, 12, pp. 4628-4641, 2006.

[2] Capmany J and Novak D, “Microwave photonics combines two worlds,” *Nat. Photonics*, vol. 1, no. 6, pp. 319, 2007.

[3] Yao J, “Microwave photonics,” *J. Light. Technol.*, vol. 27, no. 3, pp. 314-335, 2009.

[4] Ghelfi P *et al.* “Fully photonics-based coherent radar system,” *Nature*, vol. 507, no. 7492, pp. 341-345, 2014.

[5] Goda K and Jalali B, “Dispersive Fourier transformation for fast continuous single-shot measurements,” *Nat. Photonics*, vol. 7, no. 2, pp. 102-112, 2013.

[6] Jia Z, Yu J, Ellinas G, and Chang G.-K., “Key enabling technologies for optical–wireless networks: optical millimeter-wave generation, wavelength reuse, and architecture,” *J. Light. Technol.*, vol. 25, no.11, pp. 3452-3471, 2007.

[7] Koenig S *et al.*, “Wireless sub-THz communication system with high data rate,” *Nat. Photonics*, vol. 7, no.12, pp. 977981, 2013.

[8] Nagatsuma T, Ducournau G, and Renaud C C., “Advances in terahertz communications accelerated by photonics,” *Nat. Photonics*, vol. 10, no. 6, pp. 371-379, 2016.

[9] Torres‐Company V and Weiner A M, “Optical frequency comb technology for ultra‐broadband radio‐frequency photonics,” *Laser Photonics Rev.*, vol. 8, no. 3, pp. 368-393, 2014.

[10] X Zou *et al.* “Photonics for microwave measurements,” *Laser Photonics Rev.*, vol. 10, no. 5, pp. 711-734, 2016.

[11] F Zou *et al.*, “Optoelectronic oscillator for 5G wireless networks and beyond,” J. *Phys. D,* vol. 54, pp. 423002, 2021.

[12] Wikipedia. Oscillation, https://en.wikipedia.org/wiki/Oscillation

[13] Van der Pol B, “A theory of the amplitude of free and forced triode vibrations, Radio Rev. 1 (1920) 701-710, 754-762,” *Selected scientific papers* 1,1960.

[14] William F, “POST - USE REVIEW: Physics for Science and Engineering, Part I,” pp. 94-94, 1984.

[15] Yao X S and Maleki L, “High frequency optical subcarrier generator,” *Electro. Lett.*, vol.30, pp: 1525-1526, 1994.

[16] Esdale D J and Howes M J, “A reaction co-efficient approach to the design of one port negative impedance oscillators,” *IEEE Trans Microw Theory Tech.*, vol. 29, pp. 770-776, 1981.

[17] Thomson E, “Method of and means for producing alternating currents,” *US Patent*, vol. 1, pp. 630, 1893.

[18] Fleming J A, “The thermionic valve and its developments in radio-telegraphy and telephony,” *Wireless Press*, Limited, 1919.

[19] Hong S, “A history of the regeneration circuit: From invention to patent litigation,” School of Biological Sciences and Program in the History and Philosophy of Science, Seoul National University, Seoul, Korea, 2004.

[20] Armstrong E H, “Some recent developments in the audio receiver,” *Proceedings of the Institute of Radio Engineers*, vol. 3, pp. 215-238, 1915.

[21] Yao X S and Maleki L, “Optoelectronic microwave oscillator,” *J. Opt. Soc. Am. B.*, vol. 13, pp. 1725-1735, 1996.

[22] Maleki L, “The optoelectronic oscillator,” *Nat. Photonics*, vol. 5, pp. 728-730, 2011.

[23] Yao X S and Maleki L. 1996 Converting light into spectrally pure microwave oscillation. Optical Letters, **21** 483-485.

[24] Murray W *et al.* “High quality factor photonic crystal nanobeam cavities,” *Appl. Phys. Lett,* vol. 94, no. 12, 2009.

[25] Ali H, “Oscillator phase noise: A tutorial.” *IEEE J Solid-State Circuits,* vol. 35, no. 3, pp: 326-336, 2000.

[26] Robins W. P. “*Phase noise in signal sources: theory and applications*,” *IET,* Vol. 9, 1984.

[27] Yao J, “A wideband frequency tunable optoelectronic oscillator incorporating a tunable microwave photonic filter based on phase-modulation to intensity-

modulation conversion using a phase-shifted fiber Bragg grating," *IEEE Trans Microw Theory Tech*, vol. 60, no. 6, pp. 1735-1742, 2012.

[28] Zou X *et al*., "Optoelectronic oscillators (OEOs) to sensing, measurement, and detection," *IEEE J. Quantum Electron.*, vol. 52, pp. 1-16, 2015.

[29] Yao X S, Eliyahu D and Maleki L, "Progress in the opto-electronic oscillator a ten-year anniversary review," *IEEE MTT-S International Microwave Symposium Digest*, vol. 1, pp. 287-290, 2004.

[30] Eliyahu D, Seidel D and Maleki L, "Phase noise of a high performance OEO and an ultra-low noise floor cross-correlation microwave photonic homodyne system," *IEEE International Frequency Control Symposium, Honolulu, HI,* pp. 811-814, 2008.

[31] Yao X S and Maleki L. "Multiloop optoelectronic oscillator," *IEEE J Quantum Electron.*, vol. 36, pp. 79-84, 2000.

[32] Yao X S *et al*., "Dual-loop opto-electronic oscillator," In *IEEE International Frequency Control Symposium*, 1998.

[33] Zhou W and Blasche G, "Injection-locked dual opto-electronic oscillator with ultra-low phase noise and ultra-low spurious level," *IEEE Trans. Microw. Theory Tech.*, vol. 53, pp. 929-933, 2005.

[34] Okusaga O *et al*., "Spurious mode reduction in dual injection-locked optoelectronic oscillators," *Opt. Express*, vol. 19, pp. 5839-5854, 2011.

[35] Salik E, Yu N and Maleki L, "An Ultralow Phase Noise Coupled Optoelectronic Oscillator," *IEEE Photon. Technol. Lett.*, vol. 19, pp. 444–446, 2007.

[36] Yao X S, Davis L and Maleki L, "Coupled optoelectronic oscillators for generating both RF signal and optical pulses," *J. Light. Technol.*, vol. 18, pp. 73-78, 2000.

[37] Hao T *et al*., "Toward monolithic integration of OEOs: from systems to chips," *J. Light. Technol.*, vol. 36, pp. 4565-4582, 2018.

[38] Chembo Y, "Optoelectronic oscillators with time-delayed feedback," *Rev. Mod. Phys.*, vol. 91, pp. 035006, 2019.

[39] Hao T *et al*., "Recent advances in optoelectronic oscillators," *Adv. photonics*, vol. 2, pp. 044001, 2020.

[40] Peng H *et al*., “Tunable DC-60 GHz RF generation utilizing a dual-loop optoelectronic oscillator based on stimulated Brillouin scattering,” *J. Light. Technol.*, vol. 33, pp. 2707-2715, 2015.

[41] Dai J *et al*., “Super-mode noise suppression with mutual injection locking for coupled optoelectronic oscillator,” *Opt. Express*, vol. 25, pp. 27060-27066, 2017.

[42] Liu S *et al*. “Wideband Microwave Frequency Division Based on an Optoelectronic Oscillator,” *IEEE Photon. Technol. Lett.*, vol. 31, pp. 389-392, 2019.

[43] Peng H *et al.,* “Ultra-Low Phase Noise and Frequency Agile X-Band Frequency Synthesizer Based on a Phase Locked Optoelectronic Oscillator,” Joint Conference of the IEEE International Frequency Control Symposium and European Frequency and Time Forum (EFTF/IFC), Orlando, FL, USA, pp. 1-3, 2019.

[44] Chen G *et al*., “Frequency-Tunable OEO Using a DFB Laser at Period-One Oscillations with Optoelectronic Feedback,” *IEEE Photon. Technol. Lett.,* vol. 30, pp. 1593-1596, 2018.

[45] Zhu X *et al*., “Frequency-Stable Optoelectronic Oscillator Based on Passive Phase Compensation,” *IEEE Photon. Technol. Lett.,* vol. 32, pp. 612-615, 2020.

[46] Hasanuzzaman G K M, Iezekiel S and Kanno A, “W-Band Optoelectronic Oscillator,” *IEEE Photon. Technol. Lett.,* vol. 32, pp. 771-774, 2020.

[47] Li W and Yao J, A “Wideband Frequency Tunable Optoelectronic Oscillator Incorporating a Tunable Microwave Photonic Filter Based on Phase-Modulation to Intensity-Modulation Conversion Using a Phase-Shifted Fiber Bragg Grating,” *IEEE Trans. Microw. Theory Tech.*, vol. 60, pp. 1735-1742, 2012.

[48] Yu Y *et al*. “Frequency Stabilization of the Tunable Optoelectronic Oscillator Based on an Ultra-High-Q Micro-ring Resonator,” *IEEE J Quantum Electron.* vol. 26, pp. 1-9, 2020.

[49] Fan Z *et al*. “Hybrid Frequency-Tunable Parity-Time Symmetric Optoelectronic Oscillator,” *J. Light. Technol.*, vol. 38, pp. 2127-2133, 2020.

[50] Ly A *et al*., “Highly Spectrally Pure 90-GHz Signal Synthesis Using a Coupled Optoelectronic Oscillator,” *IEEE Photon. Technol. Lett.,* vol. 30, pp. 1313-1316, 2018.

[51] Yang B *et al*., “Active mode-locking optoelectronic oscillator,” *Opt. Express*, vol. 28, pp. 33220-33227, 2020.

[52] Sun T, “High-Resolution X -Band Frequency Synthesizer Using SILPLL Optoelectronic Oscillators,” IEEE Transactions on Ultrasonics, Ferroelectrics, and Frequency Control, vol. 67, pp. 217-223, 2019.

[53] Hosseini S E *et al*., “Tunable Low-Jitter Low-Drift Spurious-Free Transposed-Frequency Optoelectronic Oscillator,” *IEEE Trans. Microw. Theory Tech.*, vol. 65, pp. 72625-2635, 2017.

[54] Zhang W and Yao J, “Silicon photonic integrated optoelectronic oscillator for frequency-tunable microwave generation,” *J. Light. Technol.*, vol.36, pp. 4655-4663, 2018.

[55] Primiani P *et al.,* “Tunable optoelectronic oscillator based on an integrated heterodyne source,” IEEE International Topical Meeting on Microwave Photonics (MWP), Long Beach, CA, pp. 251-254, 2016.

[56] Zhang X *et al.,* “Simple frequency-tunable optoelectronic oscillator using integrated multi-section distributed feedback semiconductor laser,” *Opt. Express*, vol. 27, pp. 7036-7046, 2019.

[57] Zou F *et al.,* “Parity-time symmetric optoelectronic oscillator based on an integrated mode-locked laser,” *IEEE J Quantum Electron.*, vol. 57, pp. 500209, 2021.

[58] Tang J *et al.,* “Integrated optoelectronic oscillator,” *Opt. Express*, vol. 26, pp. 12257–12265, 2018.

[59] OEwaves, Pasadena, CA, USA, Hi-Q Nano Opto-Electronic Oscillator. [Online]. Available: https://oewaves.com/hi-q-nano-oeo-1

[60] Volyanskiy K *et al.,* “Compact optoelectronic microwave oscillators using ultra-high Q whispering gallery mode disk-resonators and phase modulation,” *Opt. Express*, vol. 18, pp. 22358-22363, 2010.

[61] Srinivasan S *et al.,* “Microwave generation using an integrated hybrid silicon mode-locked laser in a coupled optoelectronic oscillator configuration,” in CLEO: 2013, OSA Technical Digest (online) (Optical Society of America) CTu2G.2, 2013.

[62] Li J, Lee H and Vahala K, “Microwave synthesizer using an on-chip Brillouin oscillator,” *Nat. Commu.*, vol. 4, pp. 2097, 2013.

[63] Chen G *et al.,* “An Optoelectronic Oscillator based on Self-Injection-Locked Monolithic Integrated Dual-mode Amplified Feedback Laser,” in Asia Communications and Photonics Conference, OSA Technical Digest (online) (Optical Society of America), Su2A.10, 2017.

[64] Zhang W and Yao J, “Silicon Photonic Integrated Optoelectronic Oscillator for Frequency-Tunable Microwave Generation,” *J. Light. Technol.*, vol. 36, pp. 4655–4663, 2018.

[65] Savchenkov A A *et al.,* “Whispering-gallery mode based opto-electronic oscillators,” IEEE International Frequency Control Symposium, Newport Beach, CA, pp. 554-557, 2010.

[66] Han J *et al.,* “Wideband frequency-tunable optoelectronic oscillator with a directly modulated AlGaInAs/InP integrated twin-square micro-laser,” *Opt. Express*, vol. 26, pp. 31784-31793, 2018.

[67] Liao M *et al.,* “Narrow-linewidth microwave generation by an optoelectronic oscillator with a directly modulated micro-square laser,” *Opt. Letter*, vol. 42, pp. 4251-4254, 2017.

[68] Pollet T *et al.,* “BER sensitivity of OFDM systems to carrier frequency offset and wiener phase noise,” *IEEE Trans. Commun*., vol. 43, pp. 191-193, 1995.

[69] Meyr H, “Digital communication receivers: synchronization,” Channel Estimation and Signal Processing, 1998.

[70] Tomba L, “On the effect of Wiener phase noise in OFDM systems,” *IEEE Trans. Commun*., vol. 46, pp. 580-583, 1998.

[71] Armada A G, “Understanding the effects of phase noise in orthogonal frequency division multiplexing (OFDM),” *IEEE Trans. Broadcasting*, vol. 47, pp. 153-159, 2001.

[72] Munier F *et al.,* “Estimation of phase noise for QPSK modulation over AWGN channels,” In Proc. Giga-Hertz Symp, pp. 4-5, 2003.

[73] Wu S and Bar-Ness Y, “OFDM systems in the presence of phase noise: consequences and solutions,” *IEEE Trans. Commu*., vol. 52, pp. 1988-1996, 2004.

[74] Munier F, Eriksson T, and Svensson A. “An ICI reduction scheme for OFDM system with phase noise over fading channels,” *IEEE Trans. Commu.*, vol. 56, pp. 1119-1126, 2008.

[75] Andrews J G *et al.,* “What will 5g be?” *IEEE J. Sel. Areas Commun.*, vol. 32, pp. 1065-1082, 2014.

[76] Gupta A and Jha R K “A survey of 5g network: Architecture and emerging technologies,” *IEEE access*, vol.3, pp. 1206-1232, 2015.

[77] Lin J C “Synchronization requirements for 5g: An overview of standards and specifications for cellular networks,” *IEEE Veh. Technol. Mag.*, vol. 13, pp. 91-99, 2018.

[78] Technical Specification Group Radio Access Network 3rd Generation Partnership Project 2020-07 Study on scenarios and requirements for next generation access technologies (release 16). Document 3GPP TR 38.913 V16.0.0.

[79] Technical Speciation Group Radio Access Network 3rd Generation Partnership Project 2020-06 Nr, physical channels and modulation (release 16). 3GPP TS 38.211 V16.2.0.

[80] Maleki L, “Optoelectronic oscillator for photonic systems,” *IEEE Journal of Quantum Electronics*, vol. 32, no. 7, pp. 1141-1149, 1996.

[81] Levy E C, Horowitz M, and Menyuk C R., “Modeling optoelectronic oscillators,” *J. Opt. Soc. Am. B.*, vol. 26, pp. 148-159, 2009.

[82] Chembo Y K *et al.,* “Instabilities of microwaves generated with optoelectronic oscillators,” *Opt. Lett.*, vol. 32, pp. 2571- 2573, 2007.

[83] wikipedia.org/wiki/Electro-optic_modulator

[84] Carlos R *et al.*, “Quantum modelling of electro‐optic modulators,” *Laser Photonics Rev.,* vol. 5, no. 6, pp: 750-772, 2011.

[85] Liu K *et al.,* “Review and perspective on ultrafast wavelength‐size electro‐optic modulators.” *Laser Photonics Rev.,* vol. 9, no. 2, pp: 172-194, 2015.

[86] Emmanouil E *et al.*, “Electro-optic modulation in integrated photonics.” *J. Appl. Phys,* vol. 130, no. 1, 2021.

[87] Du S C *et al.*, “A broadband fluorographene photodetector,” *Adv. Mater.*, vol. 29, no. 22, pp.1700463, 2017.

[88] Zhao Y *et al.,* “Recent research process on perovskite photodetectors: a review for photodetector—materials, physics, and applications." *Chinese Physics B,* vol. 27, no. 12, pp: 127806, 2018.

[89] Martyniuk P *et al.,* “New concepts in infrared photodetector designs.” *Appl. Phys. Rev,* vol. 1, no. 4, 2014.

[90] Zhang H *et al.*, “A low-power, linearized, ultra-wideband LNA design technique,” *IEEE J. solid-state circuits*, vol. 44, no.2, pp. 320-330, 2009.

[91] Ortega B *et al.,* “A tutorial on microwave photonic filters,” *J. Light. Technol.*, vol. 24, no. 1, pp. 201-229, 2006.

[92] Shaman H.N., “New S-band bandpass filter (BPF) with wideband passband for wireless communication systems,” *IEEE Microw. Wirel. Compon. Lett*., vol. 22, no. 5, pp. 242-244, 2012.

[93] Cao *Z et al.*, “Reconfigurable six-section wavelength-tunable distributed Bragg reflector laser,” 2016 25th Wireless and Optical Communication Conference, (WOCC, 2016), pp.1–4, 2016.

[94] Jalili H and Momeni O, “A 230-ghz high-power and wideband coupled standing wave VCO in 65-nm CMOS,” *IEEE J. Solid-State Circuits*, vol. 55, pp. 547-556, 2020.

[95] Hao W *et al.,* “High-efficiency millimetre-wave single-ended and differential fundamental oscillators in CMOS,” *IEEE J. Solid-State Circuits,* vol. 53, pp. 1-13, 2018.

[96] Afshari E *et al.,* “A compact 275 GHz harmonic vco with -2.6 dBm output power in a 130 nm sige process,” *In 2019 IEEE Custom Integrated Circuits Conference (CICC)*, 2019.

[97] Eliyahu D *et al.*, “Optoelectronic oscillator with improved phase noise and frequency stability,” In Proceedings of the International Society for Optics and

Photonics: Photonic Integrated Systems, San Jose, CA, USA, 4998, pp.139–148, 2003.

[98] Zhang Y, Hou D and Zhao J, “Long-Term Frequency Stabilization of an Optoelectronic Oscillator Using Phase-Locked Loop,” *J. Light. Technol.*, vol. 32, pp. 2408-2414, 2014.